

Imaging the Substantia Nigra in Parkinson Disease and Other Parkinsonian Syndromes

Yun Jung Bae, MD, PhD • Jong-Min Kim, MD, PhD • Chul-Ho Sohn, MD, PhD • Ji-Hyun Choi, MD •
Byung Se Choi, MD, PhD • Yoo Sung Song, MD, PhD • Yoonho Nam, PhD • Se Jin Cho, MD •
Beomseok Jeon, MD, PhD • Jae Hyoung Kim, MD, PhD

From the Departments of Radiology (Y.J.B., B.S.C., S.J.C., J.H.K.), Neurology (J.M.K., J.H.C.), and Nuclear Medicine (Y.S.S.), Seoul National University Bundang Hospital, Seoul National University College of Medicine, 173-82 Gumi-ro, Bundang-gu, Seongnam-si, Gyeonggi-do 463-707, Republic of Korea; Departments of Radiology (C.H.S.) and Neurology (B.J.), Seoul National University Hospital, Seoul National University College of Medicine, Seoul, Republic of Korea; and Division of Biomedical Engineering, Hankyong University of Foreign Studies, Yongin, Republic of Korea (Y.N.). Received August 5, 2020; revision requested October 19; revision received November 20; accepted December 30. **Address correspondence to** J.M.K. (e-mail: jongmin1@snu.ac.kr).

Supported by a National Research Foundation of Korea grant funded by the Korean government (MSIT) (No. 2019R1F1A1063771) and the Seoul National University Bundang Hospital Research Fund (grant 09-2019-003). Y.J.B. supported by a National Research Foundation of Korea grant and the Seoul National University Bundang Hospital Research Fund. J.M.K. supported by Pepron. B.J. supported by the Seoul National University College of Medicine, Seoul National University Hospital, Sinyang Cultural Foundation, Pepron, and AbbVie Korea.

Conflicts of interest are listed at the end of this article.

Radiology 2021; 300:260–278 • <https://doi.org/10.1148/radiol.2021203341> • Content code: **NR**

Parkinson disease is characterized by dopaminergic cell loss in the substantia nigra of the midbrain. There are various imaging markers for Parkinson disease. Recent advances in MRI have enabled elucidation of the underlying pathophysiologic changes in the nigral structure. This has contributed to accurate and early diagnosis and has improved disease progression monitoring. This article aims to review recent developments in nigral imaging for Parkinson disease and other parkinsonian syndromes, including nigrosome imaging, neuromelanin imaging, quantitative iron mapping, and diffusion-tensor imaging. In particular, this article examines nigrosome imaging using 7-T MRI and 3-T susceptibility-weighted imaging. Finally, this article discusses volumetry and its clinical importance related to symptom manifestation. This review will improve understanding of recent advancements in nigral imaging of Parkinson disease.

Published under a CC BY 4.0 license.

Parkinson disease (PD) is the second most prevalent neurodegenerative disorder after Alzheimer disease (1). It is characterized by motor symptoms caused by α -synuclein-mediated dopaminergic cell loss and iron overload in the substantia nigra (SN) of the midbrain (1). Nonmotor (ie, cognitive or neuropsychiatric) symptoms can develop through other neurotransmitter systems (eg, the cholinergic, serotonergic, or noradrenergic system) (2). Symptoms of idiopathic PD can overlap with those of other movement disorders. The latter include Parkinson-plus syndromes, such as multiple system atrophy (MSA) or progressive supranuclear palsy (PSP), and other movement disorders mimicking PD, including drug-induced parkinsonism, essential tremor (ET), or vascular parkinsonism. This overlap of signs and symptoms and the scarcity of markers contribute to clinical diagnostic errors (up to 25%) and delayed or inappropriate treatment (3–5).

The traditional role of brain MRI in PD and Parkinson-plus syndromes was to support clinical diagnosis by enabling exclusion of other disease processes or to plan deep brain stimulation (6). In the early days of brain MRI for PD and Parkinson-plus syndromes, the main imaging finding observed was hypointensity in the SN and putamen with volume loss, reflecting abundant iron deposits as the result of neurodegeneration (7–10).

Recently, several advanced imaging markers have emerged as important tools in the visualization of neuroanatomic and functional processes in PD (11). MRI has progressed to reveal the neuropathologic hallmarks of PD neurodegenerative changes that affect the nigral structure. Specifically, it can be used to (a) detect characteristic PD

findings, (b) differentiate PD from other parkinsonian syndromes, and (c) monitor disease progression (12). There are currently quantitative methods with which to estimate biochemical changes in the brain, including iron deposits and/or local neuromelanin (NM) reduction and microstructural integrity (11).

This article aims to review up-to-date structural neuroimaging of the SN and its related structures in patients with PD. We examine and discuss findings on nigrosome imaging using 3- and 7-T MRI, NM imaging, quantitative iron mapping, and diffusion-tensor imaging. We also investigate the imaging findings in other parkinsonian syndromes including Parkinson-plus syndromes that should be differentiated from PD. Additionally, we review the volumetric findings to identify characteristic imaging markers associated with the clinical symptoms in PD and other parkinsonian syndromes.

Literature Search

The search was mainly performed in MEDLINE and EMBASE databases. The following search terms were used: (a) *parkinsonism, parkinsonian, Parkinson disease*; (b) *Parkinson plus syndrome, atypical parkinsonism, multiple system atrophy, progressive supranuclear palsy, essential tremor, vascular parkinsonism, drug-induced parkinsonism, dementia, Lewy bodies*; (c) *magnetic resonance imaging, nigral imaging*; (d) *nigrosome, substantia nigra*; (e) *dopamine transporter imaging, single photon emission computed tomography*; (f) *iron-sensitive, susceptibility, susceptibility weighted imaging, quantitative susceptibility mapping, relaxometry*; (g) *neuromelanin, neuromelanin imaging*; (h) *diffusion tensor imaging*.

Abbreviations

DLB = dementia with Lewy bodies, DTI = diffusion-tensor imaging, ET = essential tremor, FA = fractional anisotropy, ^{123}I -FP-CIT = iodine 123-2 β -carbomethoxy-3 β -(4-iodophenyl)-*N*-(3-fluoropropyl)-nortropane, MD = mean diffusivity, MSA = multiple system atrophy, MSA-C = MSA with predominant cerebellar ataxia, MSA-P = MSA with predominant parkinsonism, NM = neuromelanin, PD = Parkinson disease, PDD = PD with dementia, PD-MCI = PD with mild cognitive impairment, PSP = progressive supranuclear palsy, QSM = quantitative susceptibility mapping, RBD = rapid eye movement sleep behavior disorder, SN = substantia nigra, SWI = susceptibility-weighted imaging, MDS-UPDRS-III = Movement Disorder Society–Unified Parkinson Disease Rating Scale part III

Summary

This review presents up-to-date imaging applications in the substantia nigra and its related structures used in Parkinson disease and other parkinsonian syndromes, assesses their usefulness, and discusses multimodal approaches that might further improve the diagnosis and treatment of this disease.

Essentials

- Various MRI techniques can effectively elaborate on the neuroanatomic and pathophysiologic changes in the nigral structure of patients with Parkinson disease and other parkinsonian syndromes.
- Nigral imaging can be useful in diagnosing and monitoring Parkinson disease, which can be well visualized with 3- and 7-T MRI.
- Nigral imaging with a combination of different MRI techniques can provide profound information about Parkinson disease and other parkinsonian syndromes.

tractography, fractional anisotropy, diffusivity, white matter, (i) volumetry, 3D T1, cortex, gray matter, and volume. Combinations of the keywords, synonyms, and abbreviations were used for the search. Additionally, the reference lists of the retrieved articles were also searched to identify other relevant articles.

Nigrosome Imaging

Nigrosomes are three-dimensional organizations of calbindin-poor zones within calbindin-rich neuropils of the nigral complex in the SN (13). Nigrosomes can be divided into five calbindin-scarce zones, with nigrosome 1 being the largest. Nigrosome 1 is located in the ventral third and lateral two-thirds of the calbindin-rich nigral matrix. However, it is more dorsolateral at the caudal level (13). In PD, progressive dopaminergic cell loss in the SN occurs mainly in the nigrosomes, where maximal depletion occurs in nigrosome 1, followed by nigrosomes 2, 4, 3, and 5, respectively (14).

High-spatial-resolution MRI has enabled direct nigrosome visualization in the SN. By using 3- and 7-T MRI, gradient-recalled echo imaging and susceptibility-weighted imaging (SWI) reveal the detailed anatomic structure of the SN (15–28). The nigrosome 1 structure was first shown on 7-T MRI scans using T2*-weighted gradient-recalled echo imaging (16). At the level of the inferior third of the red nucleus, nigrosome 1 appears as a pocket-like hyperintense indentation at the medial aspect of the hypointense area attributed to iron deposition in the SN (20). At a more caudal level, nigral hyperintensity from nigrosome 1 appears as a linear or oval structure between the two SN hypointensity layers,

which results in a trilaminar pattern (Fig 1). The use of 3-T SWI has yielded similar nigrosome 1 findings (Fig 2, A–D) (22–28). Across the literature, different terms, such as *swallow tail sign*, *SN dorsolateral hyperintensity*, or simply *nigrosome 1*, refer to nigrosome 1 appearance.

Nigrosome Imaging in PD

On both 3- and 7-T MRI scans, patients with PD show nigral hyperintensity loss (15–28). This loss of nigral hyperintensity reflects signal hypointensity due to iron deposition associated with dopaminergic neuronal loss. When using 7-T MRI, the diagnosis of PD based on nigral hyperintensity loss compared with the healthy population has shown high diagnostic performance, with sensitivity and specificity of up to 100% (21). The diagnostic performance for PD using nigral hyperintensity loss at 3-T SWI compared with healthy control subjects varies but is generally satisfactory (22–28). Moreover, the asymmetric nigrosome involvement correlates with asymmetry in clinical motor symptoms (24,28). This variability in diagnostic performance may be due to diversity in the imaging protocols and study populations (Table). However, a meta-analysis of 3-T SWI studies on the diagnosis of PD reported sensitivity of 94.6% and specificity of 94.4%, which provide sufficient evidence for the high diagnostic performance of 3-T SWI (29). When comparing 3- and 7-T MRI of the SN, the sensitivity, specificity, and diagnostic accuracy for PD diagnosis were higher with 7-T MRI (93%, 100%, 96%, respectively) than with 3-T MRI (79%, 94%, 86%, respectively) (19).

Rapid eye movement sleep behavior disorder (RBD) is a common sleep-related symptom in patients with PD. Especially idiopathic RBD is known as the premotor disease prior to the development of synucleinopathy, such as PD or dementia with Lewy bodies (DLB) (30,31). A high rate of loss of nigral hyperintensity was observed in patients with idiopathic RBD (30,31). Bae et al (31) showed that patients with idiopathic RBD with loss of nigral hyperintensity had lower dopamine transporter uptake at SPECT than those with intact nigral signal, progressing into overt PD or DLB, suggesting that nigrosome imaging could be a marker for synucleinopathy conversion risk in premotor disease. Further studies with larger and more diverse prodromal cohorts with longitudinal follow-up will provide greater insights.

Nigrosome and Dopamine Transporter Imaging

Nigrostriatal function has traditionally been evaluated with dopamine transporter imaging, such as iodine 123-2 β -carbomethoxy-3 β -(4-iodophenyl)-*N*-(3-fluoropropyl)-nortropane (^{123}I -FP-CIT) SPECT (32,33). Previous studies reported a good positive correlation between nigrosome imaging and ^{123}I -FP-CIT SPECT on both 3- and 7-T MRI (Fig 3, A and B) (20,26). However, the two methods do not absolutely agree. Preceding nigrostriatal degeneration has been observed on ^{123}I -FP-CIT SPECT images while nigral hyperintensity is maintained on 3- and 7-T MRI scans (Fig 4, A and B) (20,26). This could lead to false-negative imaging diagnoses when based on MRI alone, and future studies are needed to establish the relationship between dopamine transporter imaging and MRI.

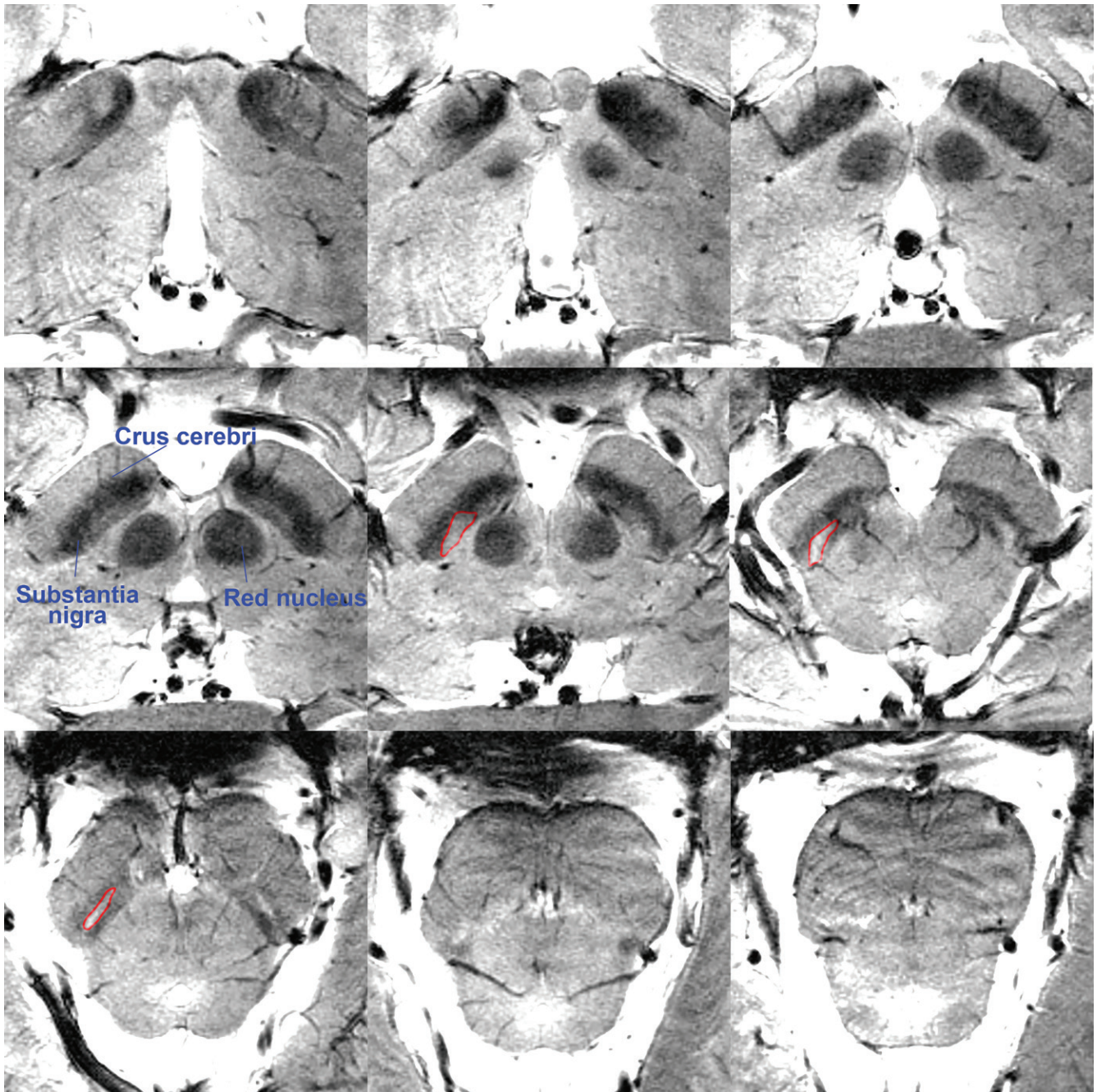


Figure 1: Normal nigra on 7-T T2*-weighted gradient-recalled echo images. Serial axial T2*-weighted gradient-recalled echo images in a 65-year-old woman obtained with 7-T MRI show bilateral hyperintensity (red outlines). Relevant anatomic structures are indicated on images. At the level of the red nucleus, bilateral hyperintensity is seen as pocketlike indentations. At a more caudal level, they appear as linear hyperintensity between two layers of substantia nigra hypointensity. This hyperintensity has been called by various terms, such as *swallow tail sign*, *nigral hyperintensity*, or *dorsal hyperintensity*.

Nigrosome Imaging in Other Parkinsonian Syndromes

In contrast to patients with PD, those with drug-induced parkinsonism, dystonic tremor, ET, psychogenic movement disorder, or vascular parkinsonism have intact nigral hyperintensity (Figs 5–7) (27,34). Nigral hyperintensity on 3-T SWI scans shows high sensitivity, specificity, and diagnostic accuracy in the differentiation of drug-induced parkinsonism from idiopathic PD (35); therefore, nigrosome imaging could help distinguish PD from these conditions.

Patients with Parkinson-plus syndromes have nigrosome structure alterations on MRI scans. Similar to patients with PD, patients with PSP and MSA may show nigral hyperintensity loss (Figs 8–11). Kim et al (20) performed 7-T T2*-weighted gradient-recalled echo imaging in patients with PSP and MSA with predominant parkinsonism (MSA-P) and found that nigral hyperintensity was lost in all patients with PSP or MSA-P. This can be explained by the neurodegeneration process in PSP and MSA-P, which involves degeneration of the nigral dopaminergic

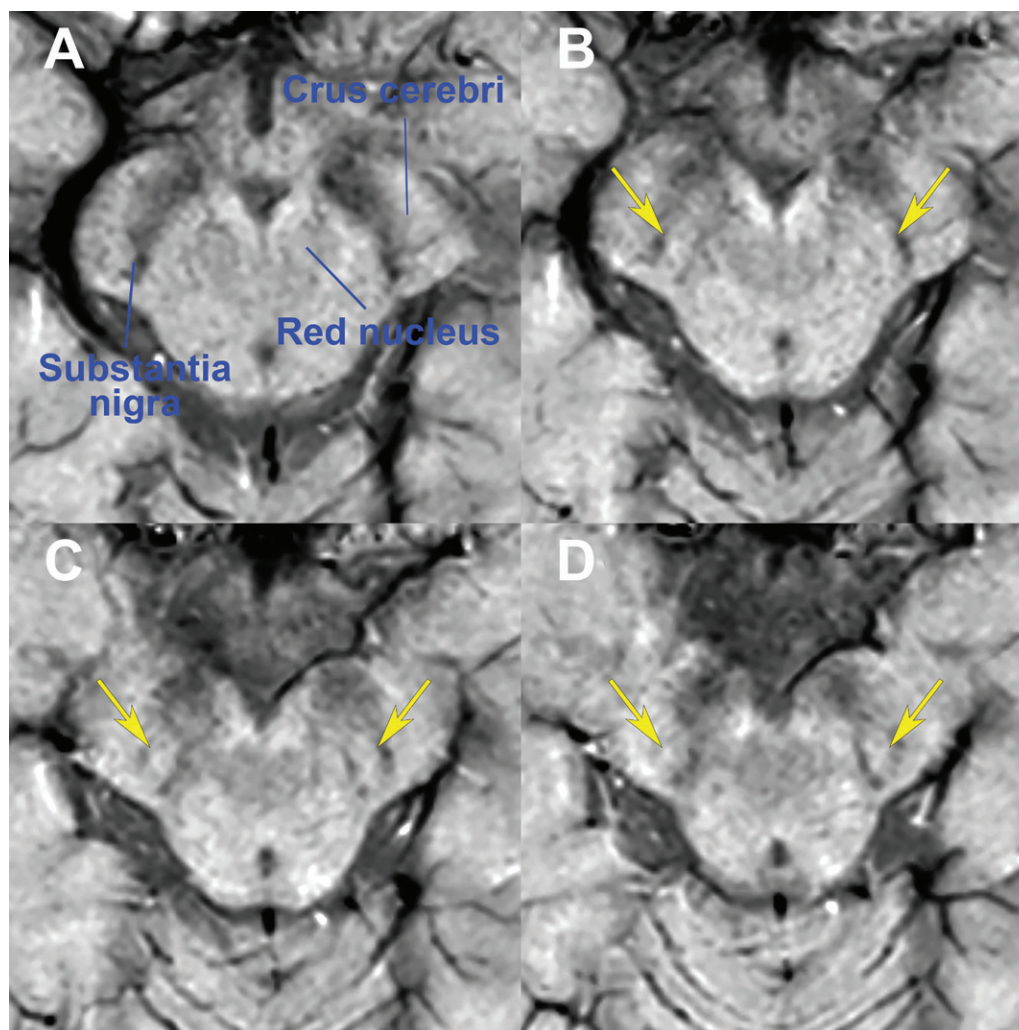


Figure 2: Normal nigra in a healthy control subject on 3-T susceptibility-weighted imaging (SWI) scans. A–D, Serial axial SWI scans in a 57-year-old woman obtained with 3-T MRI using an imaging plane vertical to the midbrain. Normal hyperintensity is observed between the two layers of the substantia nigra hypointensity (arrows).

neurons and striatonigral axons accompanying iron deposition in the SN (20). A study using 3-T SWI with a larger sample size of patients with Parkinson-plus syndromes revealed nigral hyperintensity loss in all patients with PSP, but hyperintensity was lost in only 60% of patients with MSA-P (26). Given the results of the 7-T MRI study (20), this result from the 3-T MRI study might be a false-negative finding, but future studies are warranted to verify this result. With regard to MSA with predominant cerebellar ataxia (MSA-C), only some patients (50% in the 3-T MRI study, 80% in the 7-T MRI study) showed loss of nigral hyperintensity, while the rest showed intact nigral hyperintensity. In patients with MSA-C, normal nigrostriatal dopaminergic innervation is sometimes present, which was verified by normal SPECT findings (20,26). In reflection of this finding, the status of nigral hyperintensity can be either preserved or lost in patients with MSA-C.

In addition, nigral hyperintensity can be lost in patients with DLB (36,37). However, Shams et al (36) reported many false-negative cases in patients with DLB, which can limit the role of nigral hyperintensity as a sole diagnostic test for DLB (36).

Consequently, this indicates only limited and marginal diagnostic performance for nigral hyperintensity in discriminating Parkinson-plus syndromes from PD.

Technical Improvements in Nigrosome Imaging

There have been attempts to improve the utility of nigrosome imaging with 3-T SWI. As T2*-weighted gradient-recalled echo imaging and SWI cannot effectively depict small amounts of iron, the detection of the hypointense signal change in the nigrosome 1 in such cases can be challenging. To overcome this problem, several study groups incorporated the data of the quantified local susceptibility and the phase information from the quantitative susceptibility mapping (QSM) sequence (see Quantitative Iron Mapping section) into 3-T SWI and successfully enhanced the contrast of iron-containing regions (38,39). These processed images are referred to as trueSWI (38) or susceptibility map-weighted imaging (39) according to the study groups and the detailed parameters used for image acquisition and postprocessing. Both susceptibility map-weighted imaging and trueSWI can

MRI Studies of Nigral Hyperintensity Status in Parkinson Disease

Author	Year	Field Strength (T)	Sequence	Imaging Plane	Section Thickness (mm)	Sample Size	Diagnostic Performance of Loss of Nigral Hyperintensity for PD
Cho et al (15)	2011	7	T2*-weighted GRE	AC-PC	2	9 control subjects, 10 patients with PD	All patients with PD showed serrated lateral borders of the substantia nigra
Kwon et al (16)	2012	7	T2*-weighted GRE	Oblique coronal	0.35	10 control subjects, 10 patients with PD	All patients with PD showed loss of nigral hyperintensities
Blazejewska et al (17)	2013	7	T2*-weighted image	Not specified	1	8 control subjects, 10 patients with PD	All patients with PD showed loss of nigral hyperintensities
Schwarz et al (22)	2014	3	SWI	Vertical to midbrain	0.7	90 control subjects, 19 patients with PD	Sensitivity and specificity, 100% and 95%, respectively
Cosottini et al (19)	2015	7, 3	Multiecho GRE	Vertical to midbrain	1.2 at both 3 and 7 T	13 control subjects, 14 patients with PD	7 T: sensitivity and specificity of 93% and 100%, respectively; 3 T: sensitivity and specificity of 79% and 94%, respectively
Gao et al (25)	2015	3	SWI	Vertical to midbrain	2	51 control subjects, 54 patients with PD	Sensitivity and specificity, 100% and 92.16%, respectively, for reader 1 and 98.15% and 98.04%, respectively, for reader 2
Noh et al (24)	2015	3	Multiecho GRE	Oblique coronal	1.5	13 control subjects, 24 patients with PD	Sensitivity and specificity, 100% and 84.6%, respectively
Reiter et al (23)	2015	3	SWI	Vertical to midbrain	2.4	42 control subjects, 104 patients with PD	Sensitivity and specificity, 87.5% and 92.9%, respectively (bilateral loss)
Kim et al (20)	2016	7	T2*-weighted GRE	Oblique coronal	0.35	26 control subjects, 30 patients with PD	All patients with PD showed loss of nigral hyperintensities
Bae et al (26)	2016	3	SWI	AC-PC	2	62 control subjects, 126 patients with PD	Sensitivity and specificity, 88.8% and 83.6%, respectively
Oustwani et al (27)	2017	1.5, 3	SWI	Not specified	1.6–2.25 at 1.5 T, 1.5–2.0 at 3 T	14 control subjects, 25 patients with PD	Sensitivity and specificity, 76% and 34%, respectively
Stezin et al (28)	2018	3	GRE	AC-PC	0.5 mm	63 control subjects, 67 patients with PD	Sensitivity and specificity, 98.5% and 93.6%, respectively

Note.—AC = anterior commissure, GRE = gradient-recalled echo imaging, PC = posterior commissure, PD = Parkinson disease, SWI = susceptibility-weighted imaging.

enhance nigrosome 1 visibility compared with conventional SWI in healthy control subjects (Fig 12) (38,39).

Imaging of Nigrosomes 2–5

Nigrosomes 2–5 also can be identified on high-spatial-resolution MRI scans (Fig 13) (18). Signal alterations in nigrosomes 2–5, which are affected later than nigrosome 1, have been investigated with 9.4-, 7-, and 3-T MRI (18,40,41). In particular, a study using 3-T susceptibility map-weighted imaging showed that nigrosome 4 involvement was more prevalent in late-stage PD than

in early PD (41). This confirms that nigral hyperintensity loss in PD progresses from nigrosome 1 to nigrosome 4; however, nigrosomes 2, 3, and 5 were not identified in this study. Further studies that use high-spatial-resolution MRI are necessary to reveal all nigrosome structures.

NM Imaging

NM is a protein polymer—similar to the skin pigment melanin—and a by-product of catecholamine synthesis, which is governed by the cytosolic dopamine content. It is predomi-

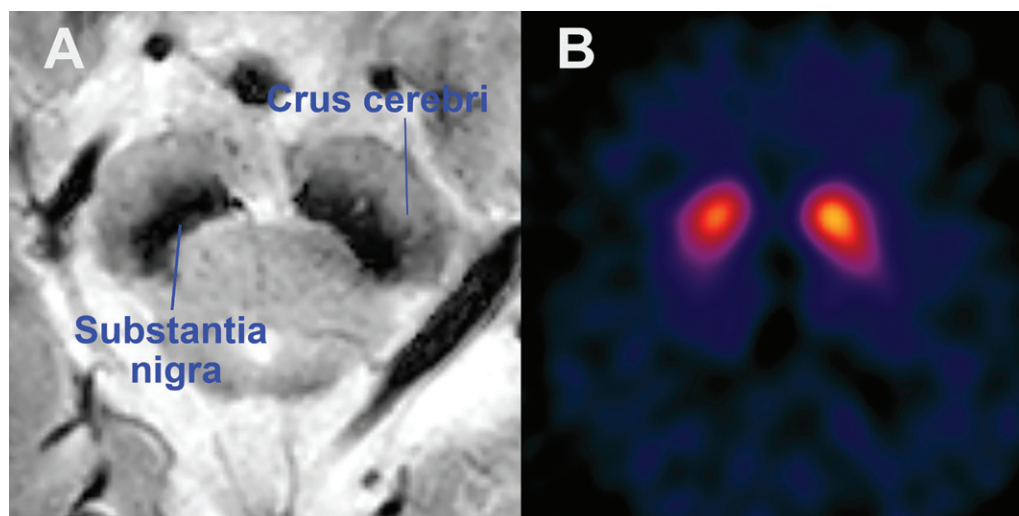


Figure 3: Abnormal nigra in Parkinson disease (PD) on 3-T susceptibility-weighted imaging scans. A, A 78-year-old man with PD presented with loss of normal nigral hyperintensity at both sides of the substantia nigra. B, Iodine 123-2 β -carbomethoxy-3 β -(4-iodophenyl)-N-(3-fluoropropyl)-nortropone SPECT scan shows correlated nigrostriatal degeneration at both striatal sides.

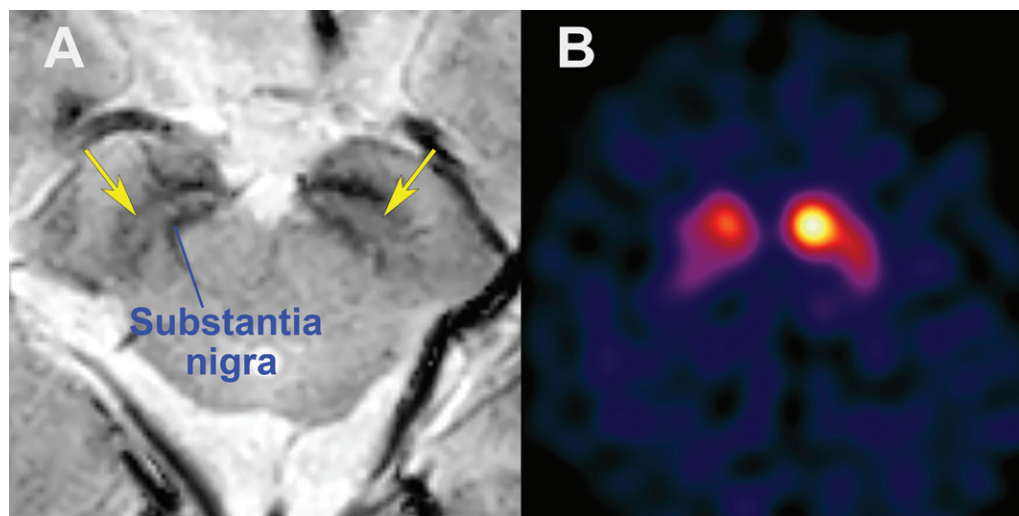


Figure 4: Discordant case of the nigral sign in a 63-year-old woman with Parkinson disease on 3-T susceptibility-weighted imaging (SWI) and iodine 123-2 β -carbomethoxy-3 β -(4-iodophenyl)-N-(3-fluoropropyl)-nortropone (^{123}I -FP-CIT) SPECT scans. A, SWI scan shows bilateral intact nigral hyperintensity of the substantia nigra (arrows). B, The ^{123}I -FP-CIT SPECT scan shows positive nigrostriatal degeneration at both sides of the basal ganglia, which suggests a precedent change in dopamine transporter imaging.

nantly located in the SN pars compacta, ventral tegmental area, and locus coeruleus (42). Neurodegeneration in PD with dopaminergic cell loss causes reduced NM-pigmented neurons, which results in depigmentation (43).

NM-sensitive MRI uses high-spatial-resolution T1-weighted imaging with fast spin-echo sequences at 3-T MRI (44,45). It is possible to obtain NM-sensitive contrast because melanin reduces T1 relaxation time, while T1 prolongation suppresses the signal from surrounding brain tissues (45). Moreover, magnetization transfer imaging can improve contrast to NM, which enhances the visualization of NM-rich areas (45). Consequently, T1 high-signal-intensity areas in the midbrain and pons represent NM-rich areas.

NM-sensitive MRI in PD

The area and contrast ratio of T1 high-signal NM pigmentation in the SN are lower in patients with PD than in healthy control subjects (Figs 14, 15) (44,46). Similar to nigrosome imaging, motor asymmetry is consistent with NM-sensitive MRI findings (47). Early PD diagnosis using NM-sensitive MRI has a sensitivity of 89% and a specificity of 85% (48). Moreover, the volume of NM-sensitive areas in the SN is negatively associated with Hoehn and Yahr staging and disease duration (44). Matsuura et al (49) evaluated the longitudinal changes in NM-sensitive MRI in patients with PD over 2 years and found that the total area and contrast ratio of the NM-prominent SN were negatively correlated with disease

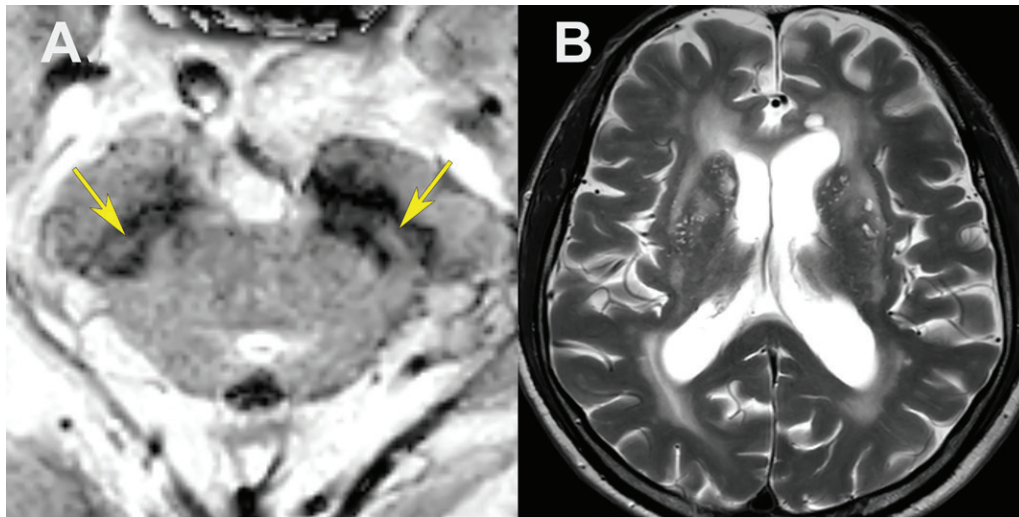


Figure 5: Images of the nigra in an 82-year-old man diagnosed with vascular parkinsonism. A, The 3-T susceptibility-weighted image shows intact bilateral nigral hyperintensity in the substantia nigra (arrows). B, Axial T2-weighted image shows a severe degree of small-vessel ischemic lesions and multiple old lacunar infarctions in both the basal ganglia and cerebral white matter.

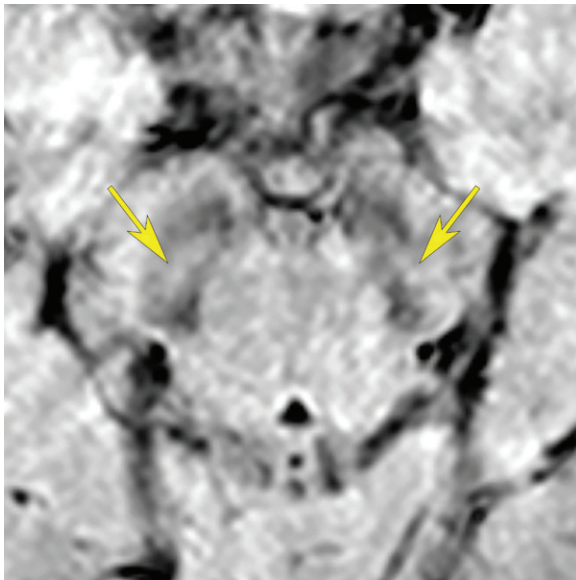


Figure 6: A 3-T susceptibility-weighted image in a 71-year-old woman diagnosed with essential tremor shows intact bilateral nigral hyperintensity in the substantia nigra (arrows).

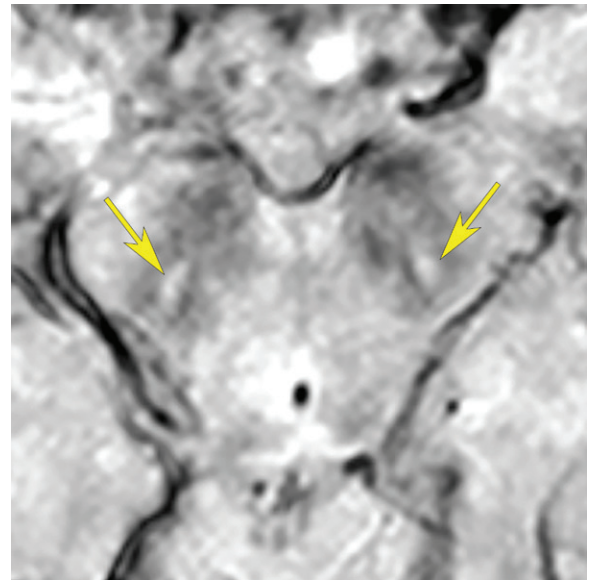


Figure 7: A 3-T susceptibility-weighted image in a 65-year-old woman diagnosed with drug-induced parkinsonism shows intact bilateral nigral hyperintensity in the substantia nigra (arrows).

duration. The size reduction of the NM-rich area was more pronounced in late stages than in early stages, progressing from lateral to central and medial SN regions (50). These findings were confirmed in a longitudinal study following a cohort of patients with PD; the volume of the SN NM content was progressively reduced with increasing disease severity, starting in the posterolateral motor areas and progressing to more medial areas (51). Interestingly, this study revealed the spatial correlation patterns between the signal-to-noise ratio of NM-sensitive MRI in distinct areas in the SN and the clinical scores as follows: (a) in the motor domain, there is a negative correlation between the NM in the bilateral posterolateral SN and Movement Disorder Society–Unified Parkinson Disease Rating Scale part III (MDS-UPDRS-III) scores; (b) in the cognitive domain, there is a positive correlation be-

tween the NM in the anteromedial and superior SN and the Mattis Dementia Rating Scale scores; and (c) in the mood and behavior domain, there is a negative correlation between the NM in the medial SN and the Arduin Scale of Behavior in Parkinson's Disease scores (51). In addition, lower signal in the locus coeruleus area can be seen not only in patients with PD with a decline in cognitive function but also in those with depression, which reflects dysfunction of the ascending noradrenergic system (52–54). Therefore, the loss in the NM-rich area can be correlated with the clinical symptoms in an anatomically localized fashion, reflecting the functional organization of the nigrostriatal system (51). A recent meta-analysis reported that NM-sensitive MRI of the SN pars compacta had a sensitivity of 82% and a specificity of 82% for PD; moreover, measuring the volume of

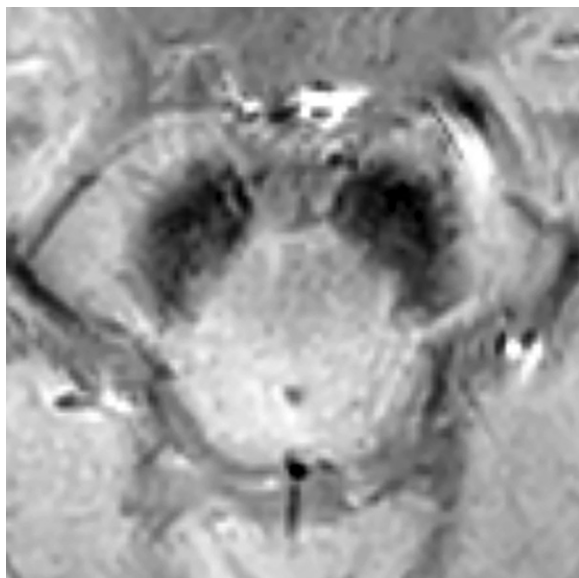


Figure 8: A 3-T susceptibility-weighted image in a 72-year-old man diagnosed with progressive supranuclear palsy shows loss of bilateral nigral hyperintensity in the substantia nigra. There are prominent iron deposits in the substantia nigra.

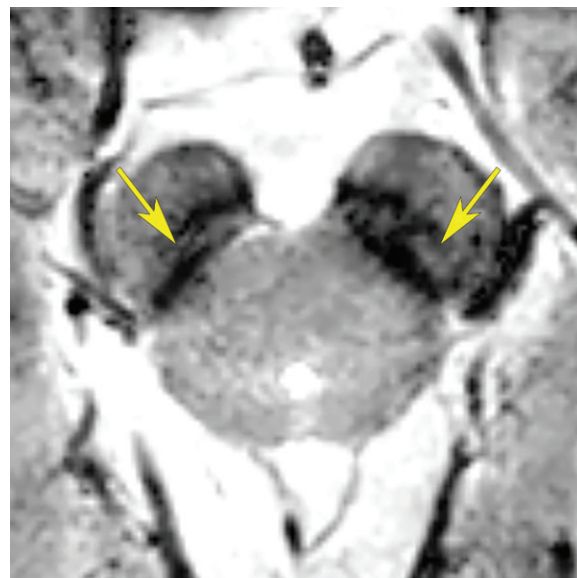


Figure 10: A 3-T susceptibility-weighted image in a 65-year-old woman diagnosed with multiple system atrophy with predominant cerebellar ataxia shows intact bilateral nigral hyperintensity in the substantia nigra (arrows).

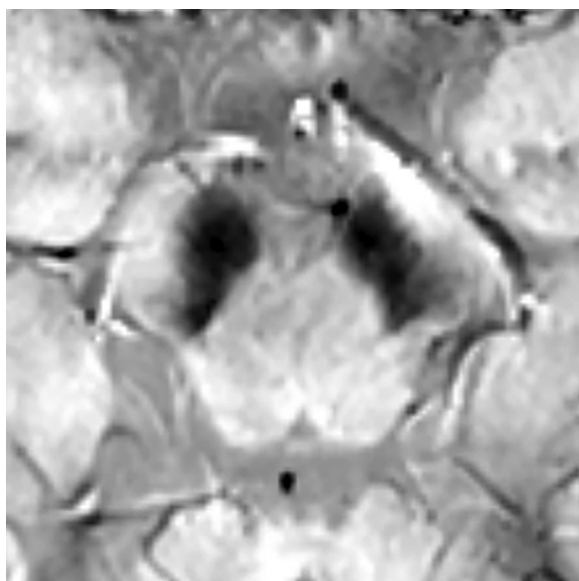


Figure 9: A 3-T susceptibility-weighted image in a 71-year-old woman diagnosed with multiple system atrophy with predominant parkinsonism shows loss of bilateral nigral hyperintensity in the substantia nigra. There are also prominent iron deposits in the substantia nigra.



Figure 11: A 3-T susceptibility-weighted image in a 61-year-old man diagnosed with multiple system atrophy with predominant cerebellar ataxia shows loss of bilateral nigral hyperintensity in the substantia nigra.

the SN pars compacta can improve the diagnostic performance (55). Given the good correlation of the NM-positive area with disease severity based on the clinical scores, NM-sensitive MRI could be an imaging marker with which to monitor nigral degeneration and disease progression (56).

Garcia-Lorenzo et al (57) have evaluated a large cohort of patients with PD using NM-sensitive MRI and found a substantial reduction of NM signal in the locus coeruleus, subcoeruleus, or both in those with RBD. Another study by Sommerauer et al (53) reported locus coeruleus NM signal decrease in patients

with PD and RBD than those with PD but without RBD, which was correlated with widespread noradrenergic impairment detected with noradrenaline transporter imaging. Future research is necessary to confirm these findings and the role of NM-sensitive MRI in the prodromal phase.

NM-sensitive MRI can allow for better delineation of the SN pars compacta and can enable more accurate examination of the hypointense signal with SWI. For instance, Langley et al (58) evaluated the iron deposition in the SN of patients with PD using hypointensity at SWI. The authors could precisely define the SN

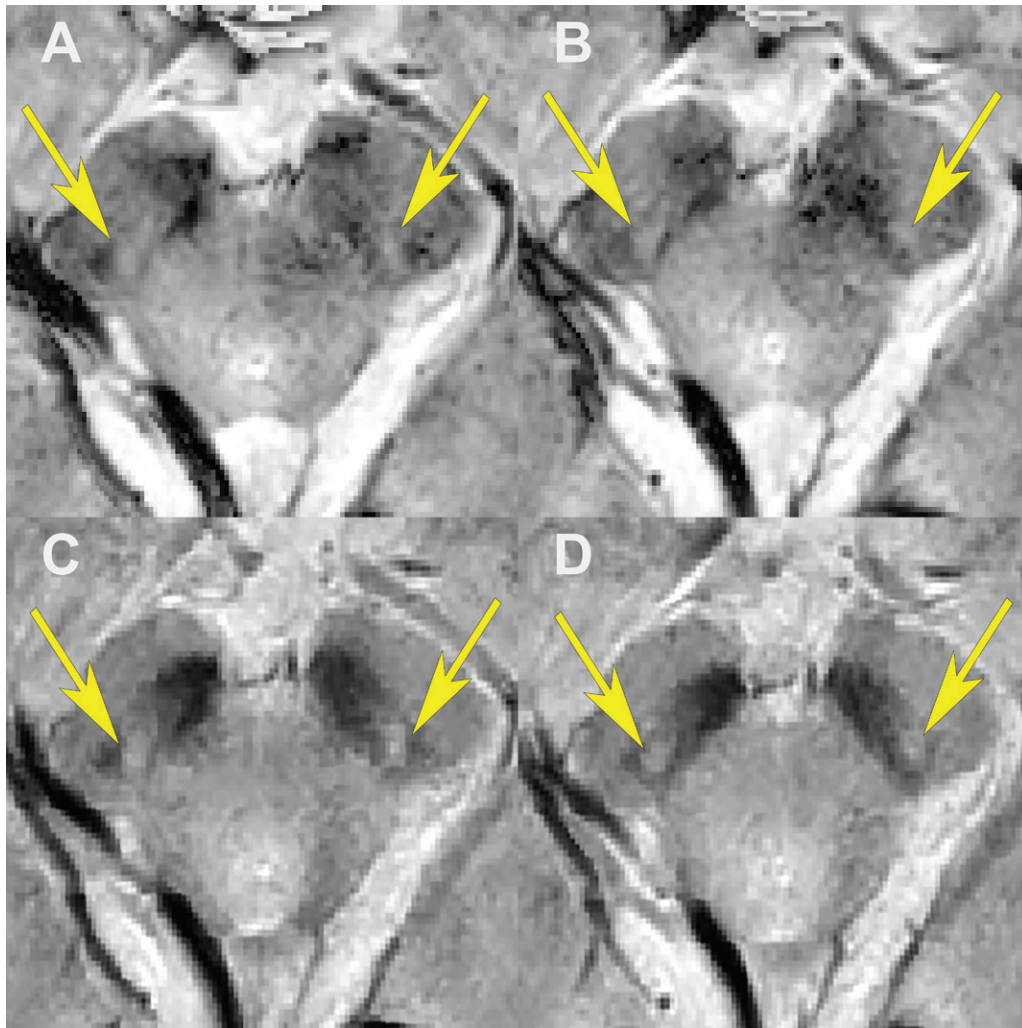


Figure 12: Comparison of susceptibility-weighted imaging (SWI) and susceptibility map-weighted imaging (SMWI) scans obtained with 3-T MRI in a 62-year-old healthy man. A, B, SWI scans show bilateral nigral hyperintensity (arrows), but images are degraded by the magnetic field–related artifact. C, D, SMWI scans show clear bilateral nigral hyperintensity with higher contrast and less artifact (arrows).

pars compacta with the help of NM-sensitive MRI. As a result, they reported that the hypointense signal on SWI is significantly increased in the SN pars compacta in patients with PD, especially in the lateral ventral region, thus, demonstrating high confidence in the combination of SWI and NM-sensitive MRI in the discrimination of patients with PD from healthy control subjects.

NM-sensitive MRI and Dopamine Transporter Imaging

The correlation between NM-sensitive MRI and ^{123}I -FP-CIT SPECT has been established. Nigral contrast ratios and NM volume on NM-sensitive MRI scans are positively correlated with striatal dopamine transporter uptake values on SPECT scans (59). A recent study reported a significant positive correlation between the NM-positive SN volume on NM-sensitive MRI scans and ^{123}I -FP-CIT uptake ratios on SPECT scans, which are both negatively correlated with the MDS-UPDRS-III score (60). Further, a multiparametric scoring system that combined NM-sensitive MRI and ^{123}I -FP-CIT SPECT scans showed comparable or better diagnostic performance than NM-sensitive

MRI or ^{123}I -FP-CIT SPECT scans alone in distinguishing PD from nondegenerative parkinsonian syndrome (61). However, the correlation between NM-sensitive MRI and dopamine transporter uptake may not be significant in the advanced PD stage. Okuzumi et al (62) found that in patients with advanced PD, clinical scores including MDS-UPDRS-III are closely associated with the size of the NM-positive SN pars compacta but not with dopamine transporter uptake.

NM-sensitive MRI in Other Parkinsonian Syndromes

When compared with healthy control subjects, patients with ET show no significant difference in NM changes in the SN on NM-sensitive MRI scans, which indicates that this technique could be used to differentiate between tremor-dominant PD and ET (63). Jin et al (64) reported the higher diagnostic performance of multimodal imaging in distinguishing ET from de novo PD. A combination of NM-sensitive MRI with nigrosome 1 imaging in the SN resulted in significantly higher diagnostic values for ET prediction.

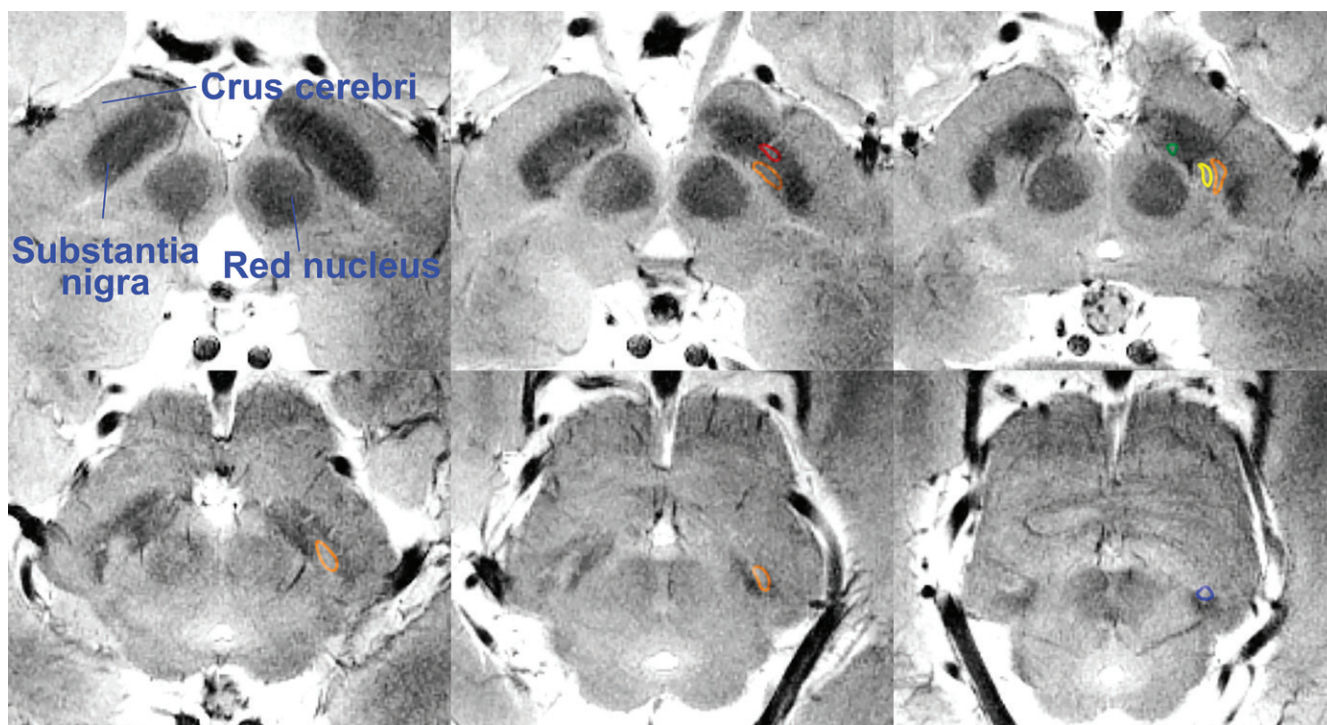


Figure 13: Serial axial 7-T T2*-weighted gradient-recalled echo images in a 61-year-old woman show the detailed structures of the nigrosomes from 1 to 5 (marked with lines on left side). The relevant anatomic structures are indicated on the images. Nigrosome 1 (orange outline) is the largest division. At the red nucleus level, nigrosome 4 (yellow outline) is located medial to nigrosome 1, and nigrosome 2 (green outline) is located anterior to nigrosome 1. Nigrosome 5 (red outline) is on the cranial side of the substantia nigra, and nigrosome 3 (blue outline) is on the caudal side of the substantia nigra.

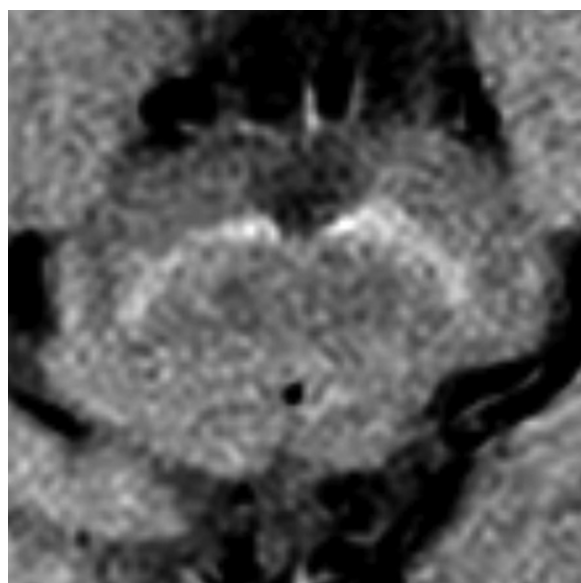


Figure 14: A 3-T neuromelanin-sensitive MRI scan in a healthy 52-year-old female control subject shows an intact area with neuromelanin-sensitive T1 high signal intensity in the substantia nigra.

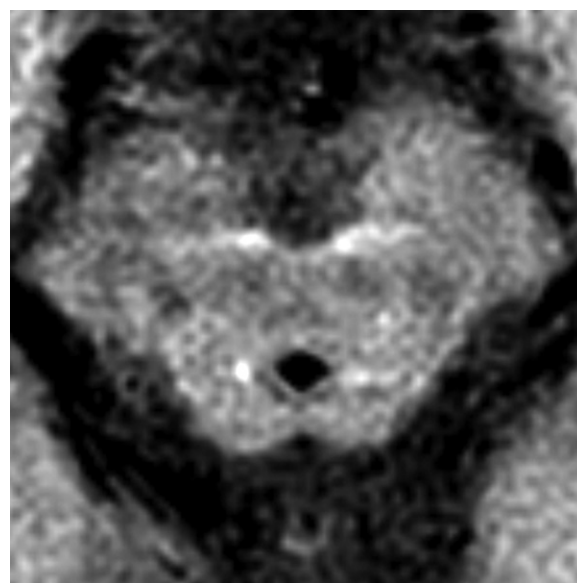


Figure 15: A 3-T neuromelanin-sensitive MRI scan in a 53-year-old male patient with Parkinson disease shows a smaller neuromelanin-sensitive T1 high-signal-intensity area than that in the healthy control subject.

Further, patients with Parkinson-plus syndromes do have changes in SN NM on NM-sensitive MRI scans. Several studies have reported volume reductions of NM-positive areas in patients with PSP and MSA (65,66). Ohtsuka et al (66) reported that evaluation of the locus coeruleus along with the SN can aid the accurate differential diagnosis between PD and Parkinson-plus syndromes. They found that the NM-positive

signal in the lateral SN was lower in patients with PD and MSA-P than in patients with PSP and healthy control subjects, and in the locus coeruleus, the signal was lower in patients with PD than in patients with MSA-P (66).

Additionally, in patients with DLB, the NM-rich areas can be reduced. An autopsy study showed that the NM-containing neurons can be lost in patients with DLB (67). Accordingly, the

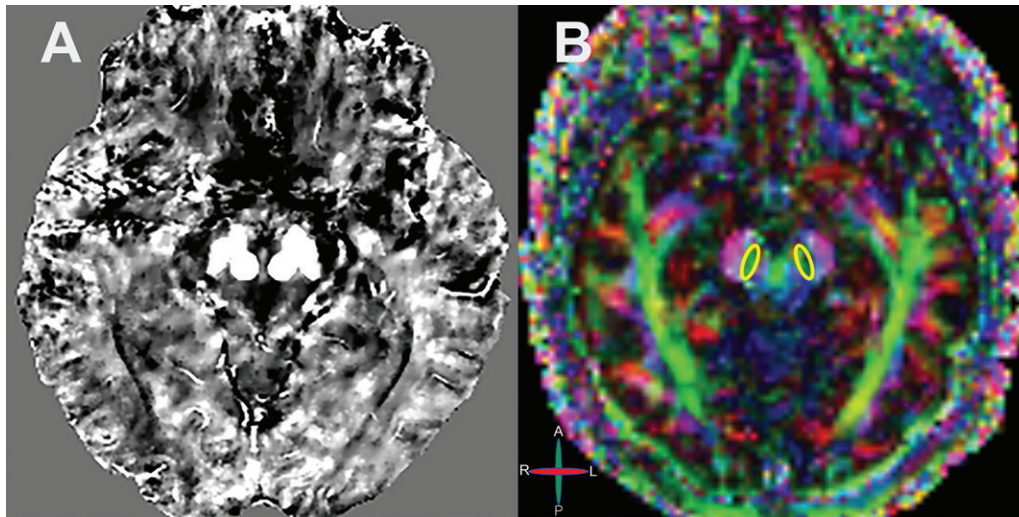


Figure 16: Examples of quantitative susceptibility mapping (QSM) and fractional anisotropy (FA) mapping from diffusion-tensor imaging in a patient with Parkinson disease (PD). A, Example of QSM in a 65-year-old man with PD shows increased susceptibility in the substantia nigra and basal ganglia (not shown) with high contrast to the surrounding tissue. B, Color-coded FA map obtained with 3-T MRI. Color bar shows the direction of the anisotropic diffusion (A, anterior; P, posterior; R, right; L, left). Regions of interest (yellow outline) are placed in the substantia nigra of the midbrain.

signal intensity of the NM-containing SN area in patients with DLB can be lower than that in healthy control subjects (67). By combining these results, NM-sensitive MRI can depict the differences among the parkinsonian syndromes. However, there is a need for future studies to further demonstrate the validity of NM-sensitive MRI in the differential diagnosis of parkinsonian syndromes.

Deep Learning Application in NM-sensitive MRI

There are various segmentation techniques to assess the NM-positive SN pars compacta, including simple manual delineation, semiautomated segmentation using a signal intensity threshold, and the atlas-based automated process (44,48,68). Recently, deep learning segmentation using convolutional neural networks based on U-net architecture has allowed the highly accurate segmentation of the SN pars compacta, comparable to that of the manual method, yielding a high performance in distinguishing patients with PD from healthy control subjects (69). Therefore, future applications of deep learning techniques are expected to support and facilitate the radiologic diagnosis of PD using NM-sensitive MRI.

Quantitative Iron Mapping

Iron is mainly stored as ferritin in the brain and alters tissue relaxation and susceptibility on MRI scans (7,10,70). Therefore, it induces signal changes in T2 or R2 ($= 1/T2$), T2* or R2* ($= 1/T2^*$), and phase values, which allows quantitative iron mapping (7,10,71). Relaxometry uses the relaxation rates of R2 and R2*, reflecting the magnetic field variance (5); however, confounding effects of other factors, including calcium, lipid, or myelin, represent limitations. On the other hand, the QSM sequence, which can be generated from the phase and magnitude data of gradient-echo or SWI sequences, can be used to objectively quantify the iron contents. Using the phase data sensitive to iron paramagnetism (72), the QSM imaging

from SWI allows effective iron quantification by converting the phase shift to the localized magnetic susceptibility (73). These sequences reflect local tissue susceptibility and macroscopic field inhomogeneities (74). Therefore, QSM sequences are known to be superior to traditional T2* or R2* relaxometry for objective iron quantification and iron-derived local susceptibility combining transverse relaxation and local field inhomogeneity (75,76) and for removing the susceptibility effect from the surrounding tissues (73,74).

Relaxometry in PD

Patients with PD show iron deposition and overload in the SN pars compacta and the striatum, with the extent correlated with disease severity measured by MDS-UPDRS-III scores (77). The R2 or R2* values can allow iron content estimation in the SN, and T2 and T2* values can be negatively correlated with iron content; therefore, R2 and R2* can show a positive correlation with iron content. Consistent with this, patients with PD have higher R2* in the SN, which has a good correlation with motor symptoms in PD, suggesting that R2* in the SN could be an imaging marker for PD progression (46,77). Patients with PD who develop freezing of gait early showed greater R2* changes in the SN pars compacta (78). Moreover, brain and serum iron levels show a positive correlation using relaxometry in patients with PD (79). This suggests that disruptions in the systemic iron metabolism affect iron partitioning in the SN. Meanwhile, several longitudinal studies assessing R2* changes over time reported controversial results. Some studies showed an increase in R2* over 2–3 years in patients with PD (77,80), while other studies reported no longitudinal changes in R2* (81,82). These findings can be partially explained by the clinical heterogeneity and wide variance of R2* (83), but further studies are needed to determine whether R2* is a promising method to monitor disease progression.

QSM in PD

As explained, in patients with PD, QSM can be used to objectively quantify iron overload in the SN pars compacta (84). A recent study showed that quantification of QSM values in nigrosomes on 3-T SWI scans was effective in the diagnosis of early PD (85). Specifically, it was shown that QSM values in the dorsolateral SN pars compacta were significantly higher in patients with PD compared with healthy control subjects with high diagnostic performance (area under the curve, 0.73) (85). Several studies have used QSM to compare the iron contents in the whole SN or the SN pars compacta between patients with PD and healthy control subjects by employing the region-of-interest approach and voxel-based analysis (Fig 16, A) (86,87). On 7-T MRI scans, susceptibility mapping by inverting the filtered phase maps associated with T2*-weighted images showed increased susceptibility caused by iron overload in the SN pars compacta in patients with PD compared with healthy control subjects (88). A more recent 3-T QSM study by Chen et al (89) reported higher magnetic susceptibility values in the SN pars compacta in patients with PD. This shows the close relationship between PD and iron deposition in the SN pars compacta. Similar findings show that QSM has a higher diagnostic performance than R2* mapping in patients with PD (74,90,91). Notably, patients with early PD showed higher susceptibility values in the bilateral SN on QSM images. However, on the R2* map, higher values only occurred in the SN contralateral to the motor-affected limb (92). This suggests that susceptibility value measurements obtained with QSM are superior to T2* or R2* relaxometry maps, especially for early PD. Nonetheless, Du et al (93) reported that QSM images in the SN pars compacta did not change over 18 months in patients with PD, while R2* did increase in patients with late-stage PD. Further studies are needed to confirm this promising method to track disease evolution.

QSM suggests regional differences in iron deposition in patients with PD. On 7-T MRI scans, there is a rostral-caudal gradient in susceptibility values along the globus pallidus and SN pathway (88). However, a recent 3-T MRI study did not report an increased iron deposition gradient along the pathways (89), indicating a need for further studies on the iron deposition mechanism in the SN. QSM studies using 3-T MRI report lateral asymmetry and posterior segment predilection in the iron deposition pattern in the SN (84). Early PD shows an exclusive increase in susceptibility values in the SN pars compacta according to the disease stage (94). However, late-stage PD shows an increase in susceptibility values in the SN pars reticulata, red nucleus, and globus pallidus, which indicates iron-related regional progression in PD. Indeed, a longitudinal study following patients with PD over 3 years revealed that longitudinal SN iron change was confined to more ventral posterior locations (95).

Susceptibility values show a correlation with clinical motor impairment and disease duration and severity. There is a significant correlation of higher susceptibility values in the red nucleus and dentate nucleus with tremor severity in patients with PD (96). Moreover, susceptibility values in the caudate nucleus are correlated with motor aspects of daily living, while susceptibility in the SN is significantly correlated with levodopa dosage and disease stages (97). In addition, nonmotor symptoms in patients

with PD also show a topographic relation to the QSM changes in the brain. QSM increase in the hippocampus and the thalamus can be associated with lower cognitive scores and QSM increase in the parietal, frontal, and medial occipital cortices can be associated with poor visual function along with a higher risk of PD with dementia (PDD) (98).

Quantitative Iron Mapping in Other Parkinsonian Syndromes

A study that performed T2* relaxometry at 3-T MRI compared the resulting values between patients with ET and healthy control subjects (99). In this study, whole-brain voxel-based analyses showed significant differences in the T2* values in the bilateral SN, bilateral globus pallidus, and right dentate nucleus. The most involved nucleus was the pallidum, which is indicative of increased iron accumulation in patients with ET and motor system involvement outside the cerebello-thalamo-cortical loop, specifically the globus pallidus, in the ET.

Patients with Parkinson-plus syndromes, including PSP and MSA, often have putaminal changes on iron-sensitive MRI scans. A postmortem pathologic study in patients with PSP, MSA, and DLB reported a significant association of R2* with nigral α -synuclein immunostaining. Moreover, QSM was significantly correlated with Perl iron staining (100). These findings suggest that quantitative iron mapping could be a valuable tool to differentiate parkinsonian syndromes and monitor the pathologic progression. Notably, patients with PSP showed higher iron concentration in the SN than did patients with MSA-P (101). Azuma et al (102) recently reported that susceptibility values in the SN were significantly higher in patients with PSP than in patients with PD and healthy control subjects.

Future Use of Quantitative Iron Mapping

Uchida et al (103) reported a significant relationship between magnetic susceptibility and dopamine transporter abnormality. They reported that patients with PD had higher QSM values in the SN than did healthy control subjects. However, there was no correlation between the QSM values in the SN and the striatal-specific binding ratios measured with ¹²³I-FP-CIT SPECT; however, there was correlation between the QSM values in the striatum and the striatal dopamine transporter density.

Recent studies have used advanced techniques, such as texture analysis or radiomics feature extraction from the SN using QSM and convolutional neural network-based feature extraction (104,105). The findings are promising, and we expect these techniques to contribute to improved diagnostic performance for PD. Although the deep learning method remains primitive, it could help identify novel imaging markers for PD.

Diffusion-Tensor Imaging

Diffusion-tensor imaging (DTI) is a technique that measures random water molecule motion in tissues (106). This allows quantification of cerebral white matter integrity, including neural fiber trajectories and orientations (107). The most common yet crucial measurements feasible with DTI are fractional anisotropy (FA) and mean diffusivity (MD) (108). FA is reflective of the orientation of the distribution of water molecular movement

(Fig 16, *B*) (106). FA is scored from 0 to 1, with 1 indicating nonuniform—anisotropic—water diffusion. Generally, the FA value in white matter is close to 1; however, the FA value gets closer to 0 in the case of damaged neural bundle integrity (106). In contrast, MD represents the diffusion of free water molecules in cerebral tissue, with its increase indicating accelerated water movement from enlarged extracellular space, which is suggestive of tissue degeneration (106). Therefore, changes in MD or FA values could reveal or measure pathologic alterations in white matter integrity (106,108). Moreover, DTI enables tractography, which enables visualization of neural pathways in the brain using the analyzed neural connectivity profile (109).

DTI in PD

Recent meta-analyses and systemic reviews show that DTI can account for structural differences in selective cerebral regions with changes in FA, MD, or both between patients with PD and healthy individuals (106,108). There have been numerous studies on FA and MD in the SN, with the majority reporting reduced FA, higher MD, or both in the region, even in patients with early PD (46,110–114). Arribarat et al (115) recently reported the concomitant increase in free water in the posterior SN with increase in $R2^*$ in the anterior SN in patients with moderate-stage PD as compared with healthy control subjects. However, findings have been inconsistent with respect to the alterations in FA and MD (116). Moreover, findings are inconsistent regarding the correlations between disease severity and FA, raising questions about the clinical importance of FA (117). However, studies using high-spatial-resolution DTI have identified greater FA reductions in the caudal SN, which allows distinction of patients with PD from control subjects with 100% sensitivity and 100% specificity (118). Several studies have combined relaxometry and DTI to increase diagnostic performance in PD (117). $R2^*$ and FA combinations in the SN and MD in the striatum allow highly accurate diagnosis of PD. Regarding longitudinal disease tracking, studies suggest that DTI changes in the SN could be used to track PD progression (113); however, the aforementioned meta-analysis by Atkinson-Clement et al (106) offers controversial conclusions.

In regard to the association of DTI measures with a patient's symptoms, findings show that DTI changes in the SN are positively correlated with the degree of bradykinesia, cognitive decline, and dopaminergic deficit (119). Chen et al (120) found that patients with PD and mild cognitive impairment (PD-MCI) have lower FA values not only in the SN but also in the diffuse white matter areas, when compared with those in patients with PD and normal cognition. Minett et al (121) also found that a higher baseline MD was related to lower attention and executive functions in patients with PD-MCI and that after longitudinal follow-up, these patients showed a significant increase in MD values in the frontal regions when compared with patients with PD and normal cognition. In addition, impaired olfactory function—one of the main nonmotor features of PD—can be associated with a trend of FA reduction and decreased volume of the olfactory tract produced by fiber tracking (122,123).

Interestingly, many authors have performed DTI-based tractography to directly visualize the nigrostriatal fiber tracts. Zhang et al (124) obtained reliable nigrostriatal tractograms in 50 patients with PD and 27 healthy control subjects but did not find significant differences between groups in the streamline numbers of the tract. However, another study using nigrostriatal tractography showed that fiber density in the nigrostriatal tract was lower in patients with PD than in healthy control subjects and even showed a negative correlation between fiber density and the MDS-UPDRS-III scores (125). This result has been reproduced by Wei et al (126), who found significantly fewer fibers passing the SN in patients with PD, which might be a potential marker for early PD when combined with reduced FA and cerebral blood flow measurements in the prefrontal cortex area. Future validation is warranted to assess nigrostriatal fiber tracts in patients with PD with further improvement in the DTI techniques.

DTI and Dopamine Transporter Imaging

A DTI study that analyzed the nigrostriatal dopaminergic pathway reported that DTI measures of the nigrostriatal tract correlate with PD severity shown by the MDS-UPDRS-III score (124). However, there was no significant correlation between DTI measures and putaminal binding ratios on dopamine transporter SPECT scans (124). There is a need for further studies to validate these findings.

DTI in Other Parkinsonian Syndromes

Prodoehl et al (112) used DTI measurements to distinguish patients with PD from healthy control subjects and from patients with ET and Parkinson-plus syndromes. The authors showed that the FA in the posterior SN was significantly higher in healthy control subjects than in patients with ET, PD, MSA-P, or PSP. FA in the posterior SN was significantly lower in patients with PD than in patients with ET, MSA-P, or PSP. Between patients with MSA-P and those with PSP, FA in the posterior caudate was lower in patients with MSA-P than in those with PSP. Further, DTI measures resulted in high diagnostic performance in distinguishing patients with PD from those with other parkinsonian syndromes (PD vs MSA-P or PSP: sensitivity, 90%; specificity, 100%; PD vs ET: sensitivity, 92%; specificity, 87%; MSA-P vs PSP: sensitivity, 90%; specificity, 100%) (112). Recently, Pyatigorskaya et al (127) used multimodal nigral imaging to discriminate patients with PSP from healthy control subjects and patients with PD. The NM-based SN volume and the FA in the midbrain were effective predictive factors to distinguish patients with PSP from healthy control subjects. In addition, the best predictors for separating PSP from PD were the NM-based SN volume and FA in the pons. This study shows that multimodal nigral imaging is a promising tool to evaluate neurodegeneration in PSP.

Lastly, many studies have assessed the presence of white matter abnormalities in patients with DLB compared with healthy control subjects or patients with other neurodegenerative diseases. Using DTI, the extensive abnormality of structural connectivity in patients with DLB has been identified, showing reduced FA in the various cerebral regions, including

the dorsal striatum, corpus callosum, amygdala, inferior longitudinal fasciculus, and frontal, parietal, and occipital regions (128–131). However, as no specific pattern has been defined, further study will be needed.

Volumetry

Structural MRI can reveal architectural changes in the brain, such as volume reduction (11). Volumetric MRI has enabled quantitative assessment of regional cerebral atrophy measured in diameters, areas, and volumes (5). The traditional measurement was based on segmentation of the region-of-interest approach, but this is operator dependent (5). Voxel-based morphometry permits operator-independent voxelwise analyses of volume differences based on coregistration of a high-spatial-resolution 3D data set, such as a magnetization-prepared rapid acquisition with gradient-echo sequence, following normalization to a study-specific template (132). It can also enable automated evaluation of the whole brain, adopting voxelwise statistical parametric mapping of preprocessed structural MRI (5,132). Furthermore, software, such as FreeSurfer and NeuroQuant, can provide fully automated segmentation into multiple neuroanatomically defined regions and can quantify regional cerebral volumes (133,134). In particular, volumetry has been extensively studied in association with clinical symptoms in PD. Here, we would like to look deeper into the volumetric findings related to the motor and nonmotor symptoms of PD, including the cognitive function in and outside of the nigral structures.

Volumetry in PD

The volume of the SN and striatum is reduced more in patients with PD than in healthy control subjects (135,136). Many studies have adopted voxel-based morphometry to measure cortical or subcortical thickness changes in patients with PD (42). When compared with healthy control subjects, patients with PD had intracranial total volume and regional volume reduction in variable cortical and subcortical sites in the brain (eg, hippocampus; amygdala; thalamus; nucleus accumbens; corpus callosum; anterior cingulate and superior temporal gyri; orbitofrontal, ventrolateral, prefrontal, and occipitoparietal cortices; and olfactory bulb) (137–141). These atrophic changes can start at an early stage of the disease (135,136). Most recently, Vitali et al (142) used 3-T magnetization transfer–prepared volumetry in patients with PD and found that the SN volume was lower in these patients than in healthy control subjects. They also found that the SN volume was even lower in patients with advanced PD than in those with de novo PD, which enables differentiation of disease stages. In regard to motor symptoms in patients with PD, a more severe tremor can be associated with cortical atrophies in the areas controlling movement sequencing, including the dorsal premotor, posterior parietal, cingulate, and left temporal cortices; and the left occipital lobe (136,143).

Volumetry and Nonmotor Symptoms in PD

PD-MCI and PDD are correlated with cerebral cortical atrophy. In a comparative study among patients with nondemented PD, PDD, or Alzheimer disease and healthy control subjects (137), those with PDD showed more significant bilateral temporal

and occipital cortical atrophy than did healthy control subjects, while patients with PD but without dementia showed only significant frontal volume reduction. Uribe et al (144) evaluated cognitive function in patients with early PD and found that cognitive and memory impairments were worse in patients with PD and posterior atrophy including the occipital and parietal gyri than in those with anterior atrophy including the orbitofrontal, anterior cingulate, and anterior temporal gyri. There has been a general consensus that, compared with PD without dementia, PD-MCI can show cortical thinning in the temporal, occipital, parietal, and supplemental motor areas, and PDD can show occipital and entorhinal cortical atrophy (145,146). Longitudinal studies have followed PD cohorts over time and have tracked the cortical changes. Filippi et al (147) observed the cortical changes in a PD cohort over 4 years and found that cortical thinning progression starts in the initial stages of cognitive decline. Another longitudinal study by Gorges et al (148) showed that although cerebral atrophy and cortical thinning including the striatum, temporoparietal regions, and primary or premotor cortex were more pronounced in cognitively impaired patients with PD, cortical brain atrophy had already expanded in patients with advanced PD even without overt cognitive deficits. Several studies have demonstrated that atrophy in the subcortical structure can be associated with cognitive function as well. Owens-Walton et al (136) found a significant correlation between greater atrophy in the caudate and poorer cognitive function and between greater atrophy in the putamen and worse motor symptoms. Another study suggested that a significant reduction in the volume of the caudate, putamen, and thalamus contributes to cognitive dysfunction (141). Particularly, for the corpus callosum, patients with PD had greater volume reduction in the corpus callosum than healthy control subjects, while patients with PDD demonstrated further reduction in the callosal volume involving multiple subsections compared with patients with PD with normal cognition or MCI (149).

Depression has been known to be associated with volume reduction in the frontal lobe, temporal lobe, amygdala, cerebellum, and left hippocampus (150–152). Isolated apathy can be correlated with precuneus degeneration, with severity positively correlated with gray matter volume in the superior frontal gyrus and cerebellar vermis (153). Regional atrophy in the frontal lobe is associated with not only cognitive impairment, but also behavioral impairment (154). Sleep disorders in patients with PD can also be related to regional cerebral atrophy; nocturnal hallucination can be related to basal ganglia atrophy, distressful dreams can be related to limbic system and frontal white matter atrophy, and nocturia can be related to volume reduction in global white matter and left pre- and postcentral cortical surface (155). Olfactory dysfunction in PD is not only correlated with olfactory bulb volume loss but also with volume loss in the left putamen, right thalamus, and right caudate nucleus (156,157).

Volumetry in Other Parkinsonian Syndromes

Extrapyramidal syndromes including ET can be differentiated from early PD with SPECT, and MRI volumetry measuring bilateral olfactory bulbs may serve as an alternative method (157).

Volumetry can play an important role in discriminating Parkinson-plus syndromes as well. Conventional MRI can demonstrate the characteristic findings of MSA including (a) atrophy of the putamen, middle cerebellar peduncle, cerebellum, or pons; (b) T2 hypointensity in the putamen and T2 hyperintense rim at dorsolateral margins of the putamen in MSA-P; and (c) the presence of T2 hyperintensity in the middle cerebellar peduncle in MSA-C (158). A meta-analysis suggested that atrophy in the putamen can be a helpful marker to distinguish MSA from PD (159). An early study has identified that volume loss in the striatum and the brainstem is more severe in patients with MSA than in patients with PD and healthy control subjects (160). It should be noted that both MSA-P and MSA-C can show volume reduction in the cerebellum and pons (160,161). In addition, volume loss in the left primary and supplemental motor area, prefrontal and insular cortex, and striatum and midbrain can be more prominent in MSA-P than in PD (162). Interestingly, patients with PDD and patients with MSA and dementia also show significant cortical thinning in the parahippocampal and lingual cortices (163).

PSP can demonstrate tegmental midbrain atrophy relative to the pons (158). A voxel-based morphometry study in patients with PSP has confirmed volume loss in the midbrain and pons, as well as in the striatum compared with that in healthy control subjects (164). Other studies have verified cortical atrophy in prefrontal and frontal, insular, and premotor and supplemental motor areas; hippocampal and parahippocampal gyrus; and subcortical and white matter atrophy in the thalamic, collicular, mesencephalic, and frontotemporal regions (165,166). When compared with patients with PD, patients with PSP also show significant volume loss in the cerebral peduncles, midbrain, and whole cerebellum (167,168). However, volumetric findings may not be a reliable method to differentiate PSP from MSA (160). For better discrimination, follow-up of volume loss over time is more necessary than the cross-sectional volumetric assessment at a single time point (169). Indeed, Reginold et al (169) performed longitudinal quantitative MRI in patients with MSA and PSP, and found that, over time, there is greater volume loss in the pons in patients with MSA, while putaminal diffusivity change is rather greater in those with PSP.

Many volumetric studies have compared DLB with Alzheimer disease. First, patients with DLB can have temporal lobe atrophy, but the degree of atrophy is less severe than that in those with Alzheimer disease (170–175). However, the differential diagnosis can be challenging in patients with mixed diseases (175,176). Some studies comparing DLB with PDD described similar involvement of the subcortical regions in both diseases (177,178). Other studies reported more decreased gray matter density in the striatum and pallidum in patients with DLB than in those with PDD (179,180), while others reported greater atrophy in the motor cortices and precuneus in patients with PDD compared with those with DLB (181). These findings should be verified in the future with longitudinal studies and a larger cohort.

Conclusion

This review presents all up-to-date nigral imaging applications used in Parkinson disease and other parkinsonian syndromes. Var-

ious advanced neuroimaging techniques using MRI have provided markers for the nigral structure to detect underlying neuroanatomic, functional, and pathophysiologic alterations. These markers can enhance diagnosis, differentiation of Parkinson disease from other movement disorders, subtyping, and disease severity monitoring. On the basis of relevant studies, we highly recommend including (a) high-spatial-resolution nigrosome 1 imaging using susceptibility-weighted imaging or its equivalent, (b) high-spatial-resolution NM-sensitive MRI, and (c) quantitative susceptibility-weighted mapping for supplementary quantitative iron mapping for nigral imaging in Parkinson disease, Parkinson-plus syndromes, and other nondegenerative parkinsonian syndromes. The use of diffusion-tensor imaging and volumetry can be supplemented according to clinical need and research purpose. There is, however, a need for further research using cutting-edge MRI technology, and multimodal imaging approaches may be necessary to identify imaging markers, improve diagnostic performance, and track the effectiveness of treatment for the disease.

Acknowledgments: We thank the National Research Foundation of Korea and the Seoul National University Bundang Hospital for research support. We also thank Editage (www.editage.co.kr) for English language editing.

Disclosures of Conflicts of Interest: Y.J.B. disclosed no relevant relationships. J.M.K. Activities related to the present article: disclosed no relevant relationships. Activities not related to the present article: received research support from Pepton. Other relationships: disclosed no relevant relationships. C.H.S. disclosed no relevant relationships. J.H.C. disclosed no relevant relationships. B.S.C. disclosed no relevant relationships. Y.S.S. disclosed no relevant relationships. Y.N. disclosed no relevant relationships. S.J.C. disclosed no relevant relationships. B.J. Activities related to the present article: disclosed no relevant relationships. Activities not related to the present article: institution received grants from Pepton and Abbvie Korea; received travel assistance from the Korea Research-Based Pharmaceutical Industry Association and the Korean Pharmaceutical Manufacturers Association. Other relationships: disclosed no relevant relationships. J.H.K. disclosed no relevant relationships.

References

- Hirtz D, Thurman DJ, Gwinn-Hardy K, Mohamed M, Chaudhuri AR, Zalutsky R. How common are the “common” neurologic disorders? *Neurology* 2007;68(5):326–337.
- Titova N, Padmakumar C, Lewis SJG, Chaudhuri KR. Parkinson's: a syndrome rather than a disease? *J Neural Transm (Vienna)* 2017;124(8):907–914.
- Hughes AJ, Daniel SE, Ben-Shlomo Y, Lees AJ. The accuracy of diagnosis of parkinsonian syndromes in a specialist movement disorder service. *Brain* 2002;125(Pt 4):861–870.
- Rajput AH, Rajput A. Accuracy of Parkinson disease diagnosis unchanged in 2 decades. *Neurology* 2014;83(5):386–387.
- Heim B, Krismer F, De Marzi R, Seppi K. Magnetic resonance imaging for the diagnosis of Parkinson's disease. *J Neural Transm (Vienna)* 2017;124(8):915–964.
- Savoirdo M. Differential diagnosis of Parkinson's disease and atypical parkinsonian disorders by magnetic resonance imaging. *Neurol Sci* 2003;24(Suppl 1):S35–S37.
- Drayer B, Burger P, Darwin R, Riederer S, Herfkens R, Johnson GA. MRI of brain iron. *AJR Am J Roentgenol* 1986;147(1):103–110.
- Pastakia B, Polinsky R, Di Chiro G, Simmons JT, Brown R, Wener L. Multiple system atrophy (Shy-Drager syndrome): MR imaging. *Radiology* 1986;159(2):499–502.
- Stern MB, Braffman BH, Skolnick BE, Hurtig HI, Grossman RI. Magnetic resonance imaging in Parkinson's disease and parkinsonian syndromes. *Neurology* 1989;39(11):1524–1526.
- Bizzi A, Brooks RA, Brunetti A, et al. Role of iron and ferritin in MR imaging of the brain: a study in primates at different field strengths. *Radiology* 1990;177(1):59–65.
- Ghadery C, Strafella AP. New imaging markers for movement disorders. *Curr Neurol Neurosci Rep* 2018;18(5):22.

12. Pyatigorskaya N, Gallea C, Garcia-Lorenzo D, Vidailhet M, Lehericy S. A review of the use of magnetic resonance imaging in Parkinson's disease. *Ther Adv Neurol Disord* 2014;7(4):206–220.
13. Damier P, Hirsch EC, Agid Y, Graybiel AM. The substantia nigra of the human brain. I. Nigrosomes and the nigral matrix, a compartmental organization based on calbindin D(28K) immunohistochemistry. *Brain* 1999;122(Pt 8):1421–1436.
14. Damier P, Hirsch EC, Agid Y, Graybiel AM. The substantia nigra of the human brain. II. Patterns of loss of dopamine-containing neurons in Parkinson's disease. *Brain* 1999;122(Pt 8):1437–1448.
15. Cho ZH, Oh SH, Kim JM, et al. Direct visualization of Parkinson's disease by in vivo human brain imaging using 7.0T magnetic resonance imaging. *Mov Disord* 2011;26(4):713–718.
16. Kwon DH, Kim JM, Oh SH, et al. Seven-Tesla magnetic resonance images of the substantia nigra in Parkinson disease. *Ann Neurol* 2012;71(2):267–277.
17. Blazejewska AI, Schwarz ST, Pitiot A, et al. Visualization of nigrosome 1 and its loss in PD: pathoanatomical correlation and in vivo 7 T MRI. *Neurology* 2013;81(6):534–540.
18. Lehericy S, Bardinet E, Poupon C, Vidailhet M, François C. 7 Tesla magnetic resonance imaging: a closer look at substantia nigra anatomy in Parkinson's disease. *Mov Disord* 2014;29(13):1574–1581.
19. Cosottini M, Frosini D, Pesaresi I, et al. Comparison of 3T and 7T susceptibility-weighted angiography of the substantia nigra in diagnosing Parkinson disease. *AJNR Am J Neuroradiol* 2015;36(3):461–466.
20. Kim JM, Jeong HJ, Bae YJ, et al. Loss of substantia nigra hyperintensity on 7 Tesla MRI of Parkinson's disease, multiple system atrophy, and progressive supranuclear palsy. *Parkinsonism Relat Disord* 2016;26:47–54.
21. Lehericy S, Vaillancourt DE, Seppi K, et al. The role of high-field magnetic resonance imaging in parkinsonian disorders: Pushing the boundaries forward. *Mov Disord* 2017;32(4):510–525.
22. Schwarz ST, Afzal M, Morgan PS, Bajaj N, Gowland PA, Auer DP. The 'swallow tail' appearance of the healthy nigrosome - a new accurate test of Parkinson's disease: a case-control and retrospective cross-sectional MRI study at 3T. *PLoS One* 2014;9(4):e93814.
23. Reiter E, Mueller C, Pinter B, et al. Dorsolateral nigral hyperintensity on 3.0T susceptibility-weighted imaging in neurodegenerative Parkinsonism. *Mov Disord* 2015;30(8):1068–1076.
24. Noh Y, Sung YH, Lee J, Kim EY. Nigrosome 1 detection at 3T MRI for the Diagnosis of early-stage idiopathic Parkinson disease: assessment of diagnostic accuracy and agreement on imaging asymmetry and clinical laterality. *AJNR Am J Neuroradiol* 2015;36(11):2010–2016.
25. Gao P, Zhou PY, Wang PQ, et al. Universality analysis of the existence of substantia nigra "swallow tail" appearance of non-Parkinson patients in 3T SWI. *Eur Rev Med Pharmacol Sci* 2016;20(7):1307–1314.
26. Bae YJ, Kim JM, Kim E, et al. Loss of nigral hyperintensity on 3 Tesla MRI of Parkinsonism: comparison with (123) I-FP-CIT SPECT. *Mov Disord* 2016;31(5):684–692.
27. Oustwani CS, Korutz AW, Lester MS, Kianirad Y, Simuni T, Hijaz TA. Can loss of the swallow tail sign help distinguish between Parkinson Disease and the Parkinson-Plus syndromes? *Clin Imaging* 2017;44:66–69.
28. Stezin A, Naduthota RM, Botta R, et al. Clinical utility of visualisation of nigrosome-1 in patients with Parkinson's disease. *Eur Radiol* 2018;28(2):718–726.
29. Mahlknecht P, Krismer F, Poewe W, Seppi K. Meta-analysis of dorsolateral nigral hyperintensity on magnetic resonance imaging as a marker for Parkinson's disease. *Mov Disord* 2017;32(4):619–623.
30. De Marzi R, Seppi K, Högl B, et al. Loss of dorsolateral nigral hyperintensity on 3.0 tesla susceptibility-weighted imaging in idiopathic rapid eye movement sleep behavior disorder. *Ann Neurol* 2016;79(6):1026–1030.
31. Bae YJ, Kim JM, Kim KJ, et al. Loss of Substantia Nigra Hyperintensity at 3.0-T MR Imaging in Idiopathic REM Sleep Behavior Disorder: Comparison with ¹²³I-FP-CIT SPECT. *Radiology* 2018;287(1):285–293.
32. Tatsch K, Poeppel G. Nigrostriatal dopamine terminal imaging with dopamine transporter SPECT: an update. *J Nucl Med* 2013;54(8):1331–1338.
33. Seibyl JP, Kupsch A, Booij J, et al. Individual-reader diagnostic performance and between-reader agreement in assessment of subjects with Parkinsonian syndrome or dementia using 123I-ioflupane injection (DaTscan) imaging. *J Nucl Med* 2014;55(8):1288–1296.
34. Perez Akly MS, Stefani CV, Ciancaglioni L, et al. Accuracy of nigrosome-1 detection to discriminate patients with Parkinson's disease and essential tremor. *Neuroradiol J* 2019;32(6):395–400.
35. Sung YH, Noh Y, Lee J, Kim EY. Drug-induced Parkinsonism versus idiopathic Parkinson disease: utility of nigrosome 1 with 3-T imaging. *Radiology* 2016;279(3):849–858.
36. Shams S, Fällmar D, Schwarz S, et al. MRI of the swallow tail sign: a useful marker in the diagnosis of Lewy body dementia? *AJNR Am J Neuroradiol* 2017;38(9):1737–1741.
37. Kamagata K, Nakatsuka T, Sakakibara R, et al. Diagnostic imaging of dementia with Lewy bodies by susceptibility-weighted imaging of nigrosomes versus striatal dopamine transporter single-photon emission computed tomography: a retrospective observational study. *Neuroradiology* 2017;59(1):89–98 [Published correction appears in *Neuroradiology* 2017;59(4):425.].
38. Cheng Z, He N, Huang P, et al. Imaging the Nigrosome 1 in the substantia nigra using susceptibility weighted imaging and quantitative susceptibility mapping: An application to Parkinson's disease. *Neuroimage Clin* 2020;25:102103.
39. Nam Y, Gho SM, Kim DH, Kim EY, Lee J. Imaging of nigrosome 1 in substantia nigra at 3T using multiecho susceptibility map-weighted imaging (SMWI). *J Magn Reson Imaging* 2017;46(2):528–536.
40. Massey LA, Miranda MA, Al-Helli O, et al. 9.4 T MR microscopy of the substantia nigra with pathological validation in controls and disease. *Neuroimage Clin* 2016;13:154–163.
41. Sung YH, Lee J, Nam Y, et al. Differential involvement of nigral subregions in idiopathic parkinson's disease. *Hum Brain Mapp* 2018;39(1):542–553.
42. Rispoli V, Schreglmann SR, Bhatia KP. Neuroimaging advances in Parkinson's disease. *Curr Opin Neurol* 2018;31(4):415–424.
43. Gibb WR, Lees AJ. Anatomy, pigmentation, ventral and dorsal subpopulations of the substantia nigra, and differential cell death in Parkinson's disease. *J Neurol Neurosurg Psychiatry* 1991;54(5):388–396.
44. Kashiwara K, Shinya T, Higaki F. Neuromelanin magnetic resonance imaging of nigral volume loss in patients with Parkinson's disease. *J Clin Neurosci* 2011;18(8):1093–1096.
45. Martin-Bastida A, Pietracupa S, Piccini P. Neuromelanin in parkinsonian disorders: an update. *Int J Neurosci* 2017;127(12):1116–1123.
46. Lehericy S, Sharman MA, Dos Santos CL, Paquin R, Gallea C. Magnetic resonance imaging of the substantia nigra in Parkinson's disease. *Mov Disord* 2012;27(7):822–830.
47. Prasad S, Saini J, Yadav R, Pal PK. Motor asymmetry and neuromelanin imaging: Concordance in Parkinson's disease. *Parkinsonism Relat Disord* 2018;53:28–32.
48. Ogisu K, Kudo K, Sasaki M, et al. 3D neuromelanin-sensitive magnetic resonance imaging with semi-automated volume measurement of the substantia nigra pars compacta for diagnosis of Parkinson's disease. *Neuroradiology* 2013;55(6):719–724.
49. Matsuura K, Maeda M, Tabei KI, et al. A longitudinal study of neuromelanin-sensitive magnetic resonance imaging in Parkinson's disease. *Neurosci Lett* 2016;633:112–117.
50. Ohtsuka C, Sasaki M, Konno K, et al. Changes in substantia nigra and locus coeruleus in patients with early-stage Parkinson's disease using neuromelanin-sensitive MR imaging. *Neurosci Lett* 2013;541:93–98.
51. Biondetti E, Gaurav R, Yahia-Cherif L, et al. Spatiotemporal changes in substantia nigra neuromelanin content in Parkinson's disease. *Brain* 2020;143(9):2757–2770.
52. Wang J, Li Y, Huang Z, et al. Neuromelanin-sensitive magnetic resonance imaging features of the substantia nigra and locus coeruleus in de novo Parkinson's disease and its phenotypes. *Eur J Neurol* 2018;25(7):949–e73.
53. Sommerauer M, Fedorova TD, Hansen AK, et al. Evaluation of the noradrenergic system in Parkinson's disease: an 11C-MeNER PET and neuromelanin MRI study. *Brain* 2018;141(2):496–504.
54. Li Y, Wang C, Wang J, et al. Mild cognitive impairment in de novo Parkinson's disease: A neuromelanin MRI study in locus coeruleus. *Mov Disord* 2019;34(6):884–892.
55. Wang X, Zhang Y, Zhu C, et al. The diagnostic value of SNpc using NM-MRI in Parkinson's disease: meta-analysis. *Neurosci* 2019;40(12):2479–2489 [Published correction appears in *Neurosci* 2019;40(12):2491.].
56. Fabbri M, Reimão S, Carvalho M, et al. Substantia nigra neuromelanin as an imaging biomarker of disease progression in Parkinson's disease. *J Parkinson Dis* 2017;7(3):491–501.
57. García-Lorenzo D, Longo-Dos Santos C, Ewencyk C, et al. The coeruleus/subcoeruleus complex in rapid eye movement sleep behaviour disorders in Parkinson's disease. *Brain* 2013;136(Pt 7):2120–2129.
58. Langley J, Huddleston DE, Sedlacik J, Boelmans K, Hu XP. Parkinson's disease-related increase of T2*-weighted hypointensity in substantia nigra pars compacta. *Mov Disord* 2017;32(3):441–449.
59. Isaias IU, Trujillo P, Summers P, et al. Neuromelanin imaging and dopaminergic loss in Parkinson's disease. *Front Aging Neurosci* 2016;8:196.

60. Kuya K, Ogawa T, Shinohara Y, et al. Evaluation of Parkinson's disease by neuromelanin-sensitive magnetic resonance imaging and ¹²³I-FP-CIT SPECT. *Acta Radiol* 2018;59(5):593–598.
61. Matsusue E, Fujihara Y, Tanaka K, et al. The utility of the combined use of ¹²³I-FP-CIT SPECT and neuromelanin MRI in differentiating Parkinson's disease from other parkinsonian syndromes. *Acta Radiol* 2019;60(2):230–238.
62. Okuzumi A, Hatano T, Kamagata K, et al. Neuromelanin or DaT-SPECT: which is the better marker for discriminating advanced Parkinson's disease? *Eur J Neurol* 2019;26(11):1408–1416.
63. Wang J, Huang Z, Li Y, et al. Neuromelanin-sensitive MRI of the substantia nigra: An imaging biomarker to differentiate essential tremor from tremor-dominant Parkinson's disease. *Parkinsonism Relat Disord* 2019;58:3–8.
64. Jin L, Wang J, Wang C, et al. Combined visualization of nigrosome-1 and neuromelanin in the substantia nigra using 3T MRI for the differential diagnosis of essential tremor and de novo Parkinson's disease. *Front Neurol* 2019;10:100.
65. Matsuura K, Maeda M, Yata K, et al. Neuromelanin magnetic resonance imaging in Parkinson's disease and multiple system atrophy. *Eur Neurol* 2013;70(1-2):70–77.
66. Ohtsuka C, Sasaki M, Konno K, et al. Differentiation of early-stage parkinsonisms using neuromelanin-sensitive magnetic resonance imaging. *Parkinsonism Relat Disord* 2014;20(7):755–760.
67. Kitao S, Matsusue E, Fujii S, et al. Correlation between pathology and neuromelanin MR imaging in Parkinson's disease and dementia with Lewy bodies. *Neuroradiology* 2013;55(8):947–953 [Published correction appears in *Neuroradiology* 2017;59(6):637–638].
68. Safai A, Prasad S, Chougule T, Saini J, Pal PK, Ingalhaliker M. Microstructural abnormalities of substantia nigra in Parkinson's disease: A neuromelanin sensitive MRI atlas based study. *Hum Brain Mapp* 2020;41(5):1323–1333.
69. Le Berre A, Kamagata K, Otsuka Y, et al. Convolutional neural network-based segmentation can help in assessing the substantia nigra in neuromelanin MRI. *Neuroradiology* 2019;61(12):1387–1395.
70. Guan X, Xu X, Zhang M. Region-specific iron measured by MRI as a biomarker for Parkinson's disease. *Neurosci Bull* 2017;33(5):561–567.
71. Langkammer C, Krebs N, Goessler W, et al. Quantitative MR imaging of brain iron: a postmortem validation study. *Radiology* 2010;257(2):455–462.
72. de Rochefort L, Liu T, Kressler B, et al. Quantitative susceptibility map reconstruction from MR phase data using bayesian regularization: validation and application to brain imaging. *Magn Reson Med* 2010;63(1):194–206.
73. Liu C, Li W, Tong KA, Yeom KW, Kuzminski S. Susceptibility-weighted imaging and quantitative susceptibility mapping in the brain. *J Magn Reson Imaging* 2015;42(1):23–41.
74. Du G, Liu T, Lewis MM, et al. Quantitative susceptibility mapping of the midbrain in Parkinson's disease. *Mov Disord* 2016;31(3):317–324.
75. Haacke EM, Xu Y, Cheng YC, Reichenbach JR. Susceptibility weighted imaging (SWI). *Magn Reson Med* 2004;52(3):612–618.
76. Wang Y, Butros SR, Shuai X, et al. Different iron-deposition patterns of multiple system atrophy with predominant parkinsonism and idiopathic Parkinson diseases demonstrated by phase-corrected susceptibility-weighted imaging. *AJNR Am J Neuroradiol* 2012;33(2):266–273.
77. Ulla M, Bonny JM, Ouchchane L, Rieu I, Claise B, Durif F. Is R2* a new MRI biomarker for the progression of Parkinson's disease? A longitudinal follow-up. *PLoS One* 2013;8(3):e57904.
78. Wieler M, Gee M, Camicioli R, Martin WR. Freezing of gait in early Parkinson's disease: Nigral iron content estimated from magnetic resonance imaging. *J Neurol Sci* 2016;361:87–91.
79. Costa-Mallen P, Gatenby C, Friend S, et al. Brain iron concentrations in regions of interest and relation with serum iron levels in Parkinson disease. *J Neurol Sci* 2017;378:38–44.
80. Hopes L, Grolez G, Moreau C, et al. Magnetic resonance imaging features of the nigrostriatal system: biomarkers of Parkinson's disease stages? *PLoS One* 2016;11(4):e0147947.
81. Rossi ME, Ruottinen H, Saunamäki T, Elovaara I, Dastidar P. Imaging brain iron and diffusion patterns: a follow-up study of Parkinson's disease in the initial stages. *Acad Radiol* 2014;21(1):64–71.
82. Wieler M, Gee M, Martin WR. Longitudinal midbrain changes in early Parkinson's disease: iron content estimated from R2*/MRI. *Parkinsonism Relat Disord* 2015;21(3):179–183.
83. Yang J, Burciu RG, Vaillancourt DE. Longitudinal progression markers of Parkinson's Disease: current view on structural imaging. *Curr Neurol Neurosci Rep* 2018;18(12):83.
84. Azuma M, Hirai T, Yamada K, et al. Lateral asymmetry and spatial difference of iron deposition in the substantia nigra of patients with Parkinson disease measured with quantitative susceptibility mapping. *AJNR Am J Neuroradiol* 2016;37(5):782–788.
85. Takahashi H, Watanabe Y, Tanaka H, et al. Quantifying changes in nigrosomes using quantitative susceptibility mapping and neuromelanin imaging for the diagnosis of early-stage Parkinson's disease. *Br J Radiol* 2018; 91(1086):20180037.
86. Acosta-Cabronero J, Cardenas-Blanco A, Betts MJ, et al. The whole-brain pattern of magnetic susceptibility perturbations in Parkinson's disease. *Brain* 2017;140(1):118–131.
87. Sjöström H, Granberg T, Westman E, Svenningsson P. Quantitative susceptibility mapping differentiates between parkinsonian disorders. *Parkinsonism Relat Disord* 2017;44:51–57.
88. Lotfipour AK, Wharton S, Schwarz ST, et al. High resolution magnetic susceptibility mapping of the substantia nigra in Parkinson's disease. *J Magn Reson Imaging* 2012;35(1):48–55.
89. Chen Q, Chen Y, Zhang Y, et al. Iron deposition in Parkinson's disease by quantitative susceptibility mapping. *BMC Neurosci* 2019;20(1):23.
90. Murakami Y, Kakeda S, Watanabe K, et al. Usefulness of quantitative susceptibility mapping for the diagnosis of Parkinson disease. *AJNR Am J Neuroradiol* 2015;36(6):1102–1108.
91. Cheng Q, Huang J, Liang J, et al. Evaluation of abnormal iron distribution in specific regions in the brains of patients with Parkinson's disease using quantitative susceptibility mapping and R2' mapping. *Exp Ther Med* 2020;19(6):3778–3786.
92. He N, Ling H, Ding B, et al. Region-specific disturbed iron distribution in early idiopathic Parkinson's disease measured by quantitative susceptibility mapping. *Hum Brain Mapp* 2015;36(11):4407–4420.
93. Du G, Lewis MM, Sica C, et al. Distinct progression pattern of susceptibility MRI in the substantia nigra of Parkinson's patients. *Mov Disord* 2018;33(9):1423–1431.
94. Guan X, Xuan M, Gu Q, et al. Regionally progressive accumulation of iron in Parkinson's disease as measured by quantitative susceptibility mapping. *NMR Biomed* 2017;30(4):e3489.
95. Bergsland N, Zivadinov R, Schweser F, Hagemeyer J, Lichter D, Guttuso T Jr. Ventral posterior substantia nigra iron increases over 3 years in Parkinson's disease. *Mov Disord* 2019;34(7):1006–1013.
96. Guan X, Xuan M, Gu Q, et al. Influence of regional iron on the motor impairments of Parkinson's disease: A quantitative susceptibility mapping study. *J Magn Reson Imaging* 2017;45(5):1335–1342.
97. Langkammer C, Pirpamer L, Seiler S, et al. Quantitative susceptibility mapping in Parkinson's disease. *PLoS One* 2016;11(9):e0162460.
98. Thomas GEC, Leyland LA, Schrag AE, Lees AJ, Acosta-Cabronero J, Weil RS. Brain iron deposition is linked with cognitive severity in Parkinson's disease. *J Neurol Neurosurg Psychiatry* 2020;91(4):418–425.
99. Novellino F, Cherubini A, Chiriaco C, et al. Brain iron deposition in essential tremor: a quantitative 3-Tesla magnetic resonance imaging study. *Mov Disord* 2013;28(2):196–200.
100. Lewis MM, Du G, Baccon J, et al. Susceptibility MRI captures nigral pathology in patients with parkinsonian syndromes. *Mov Disord* 2018;33(9):1432–1439.
101. Han YH, Lee JH, Kang BM, et al. Topographical differences of brain iron deposition between progressive supranuclear palsy and parkinsonian variant multiple system atrophy. *J Neurol Sci* 2013;325(1-2):29–35.
102. Azuma M, Hirai T, Nakaura T, et al. Combining quantitative susceptibility mapping to the morphometric index in differentiating between progressive supranuclear palsy and Parkinson's disease. *J Neurol Sci* 2019;406:116443.
103. Uchida Y, Kan H, Sakurai K, et al. Magnetic susceptibility associates with dopaminergic deficits and cognition in Parkinson's disease. *Mov Disord* 2020;35(8):1396–1405.
104. Li G, Zhai G, Zhao X, et al. 3D texture analyses within the substantia nigra of Parkinson's disease patients on quantitative susceptibility maps and R2' maps. *Neuroimage* 2019;188:465–472.
105. Sun J, Lai Z, Ma J, et al. Quantitative evaluation of iron content in idiopathic rapid eye movement sleep behavior disorder. *Mov Disord* 2020;35(3):478–485.
106. Atkinson-Clement C, Pinto S, Eusebio A, Coulon O. Diffusion tensor imaging in Parkinson's disease: Review and meta-analysis. *Neuroimage Clin* 2017;16:98–110.
107. Le Bihan D. Looking into the functional architecture of the brain with diffusion MRI. *Nat Rev Neurosci* 2003;4(6):469–480.
108. Basser PJ, Pierpaoli C. Microstructural and physiological features of tissues elucidated by quantitative-diffusion-tensor MRI. *J Magn Reson B* 1996;111(3):209–219.
109. Mori S, van Zijl PC. Fiber tracking: principles and strategies - a technical review. *NMR Biomed* 2002;15(7-8):468–480.
110. Rollheiser TM, Fulton HG, Good KP, et al. Diffusion tensor imaging and olfactory identification testing in early-stage Parkinson's disease. *J Neurol* 2011;258(7):1254–1260.

111. Prakash BD, Sitoh YY, Tan LC, Au WL. Asymmetrical diffusion tensor imaging indices of the rostral substantia nigra in Parkinson's disease. *Parkinsonism Relat Disord* 2012;18(9):1029–1033.
112. Prodoehl J, Li H, Planetta PJ, et al. Diffusion tensor imaging of Parkinson's disease, atypical parkinsonism, and essential tremor. *Mov Disord* 2013;28(13):1816–1822.
113. Loane C, Politis M, Kefalopoulou Z, et al. Aberrant nigral diffusion in Parkinson's disease: A longitudinal diffusion tensor imaging study. *Mov Disord* 2016;31(7):1020–1026.
114. Kamagata K, Hatano T, Okuzumi A, et al. Neurite orientation dispersion and density imaging in the substantia nigra in idiopathic Parkinson disease. *Eur Radiol* 2016;26(8):2567–2577.
115. Arribarat G, Pasternak O, De Barros A, Galitzky M, Rascol O, Péran P. Substantia nigra locations of iron-content, free-water and mean diffusivity abnormalities in moderate stage Parkinson's disease. *Parkinsonism Relat Disord* 2019;65:146–152.
116. Menke RA, Jbabdi S, Miller KL, Matthews PM, Zarei M. Connectivity-based segmentation of the substantia nigra in human and its implications in Parkinson's disease. *Neuroimage* 2010;52(4):1175–1180.
117. Du G, Lewis MM, Styner M, et al. Combined R2* and diffusion tensor imaging changes in the substantia nigra in Parkinson's disease. *Mov Disord* 2011;26(9):1627–1632.
118. Vaillancourt DE, Spraker MB, Prodoehl J, et al. High-resolution diffusion tensor imaging in the substantia nigra of de novo Parkinson disease. *Neurology* 2009;72(16):1378–1384 [Published correction appears in *Neurology* 2009;72(23):2059].
119. Ofori E, Pasternak O, Planetta PJ, et al. Longitudinal changes in free-water within the substantia nigra of Parkinson's disease. *Brain* 2015;138(Pt 8):2322–2331.
120. Chen F, Wu T, Luo Y, et al. Amnesic mild cognitive impairment in Parkinson's disease: White matter structural changes and mechanisms. *PLoS One* 2019;14(12):e0226175.
121. Minett T, Su L, Mak E, et al. Longitudinal diffusion tensor imaging changes in early Parkinson's disease: ICICLE-PD study. *J Neurol* 2018;265(7):1528–1539.
122. Georgiopoulos C, Wartjes M, Dizdar N, et al. Olfactory impairment in Parkinson's disease studied with diffusion tensor and magnetization transfer imaging. *J Parkinsons Dis* 2017;7(2):301–311.
123. Nigro P, Chiappinello A, Simoni S, et al. Changes of olfactory tract in Parkinson's disease: a DTI tractography study. *Neuroradiology* 2021;63(2):235–242.
124. Zhang Y, Wu IW, Buckley S, et al. Diffusion tensor imaging of the nigrostriatal fibers in Parkinson's disease. *Mov Disord* 2015;30(9):1229–1236.
125. Tan WQ, Yeoh CS, Rumpel H, et al. Deterministic tractography of the nigrostriatal-nigropallidal pathway in Parkinson's disease. *Sci Rep* 2015;5(1):17283.
126. Wei X, Yan R, Chen Z, et al. Combined Diffusion Tensor Imaging and Arterial Spin Labeling as Markers of Early Parkinson's disease. *Sci Rep* 2016;6(1):33762.
127. Pyatigorskaya N, Yahia-Cherif L, Gaurav R, et al. Multimodal magnetic resonance imaging quantification of brain changes in progressive supranuclear palsy. *Mov Disord* 2020;35(1):161–170.
128. Bozzali M, Falini A, Cercignani M, et al. Brain tissue damage in dementia with Lewy bodies: an in vivo diffusion tensor MRI study. *Brain* 2005;128(Pt 7):1595–1604.
129. Kantarci K, Avula R, Senjem ML, et al. Dementia with Lewy bodies and Alzheimer disease: neurodegenerative patterns characterized by DTI. *Neurology* 2010;74(22):1814–1821.
130. Watson R, Blamire AM, Colloby SJ, et al. Characterizing dementia with Lewy bodies by means of diffusion tensor imaging. *Neurology* 2012;79(9):906–914.
131. Delli Pizzi S, Franciotti R, Taylor JP, et al. Structural connectivity is differently altered in dementia with Lewy body and Alzheimer's disease. *Front Aging Neurosci* 2015;7:208.
132. Ashburner J, Friston KJ. Voxel-based morphometry—the methods. *Neuroimage* 2000;11(6 Pt 1):805–821.
133. Fischl B, Dale AM. Measuring the thickness of the human cerebral cortex from magnetic resonance images. *Proc Natl Acad Sci U S A* 2000;97(20):11050–11055.
134. Messina D, Cerasa A, Condino F, et al. Patterns of brain atrophy in Parkinson's disease, progressive supranuclear palsy and multiple system atrophy. *Parkinsonism Relat Disord* 2011;17(3):172–176.
135. Pitcher TL, Melzer TR, Macaskill MR, et al. Reduced striatal volumes in Parkinson's disease: a magnetic resonance imaging study. *Transl Neurodegener* 2012;1(1):17.
136. Owens-Walton C, Jakabek D, Li X, et al. Striatal changes in Parkinson disease: An investigation of morphology, functional connectivity and their relationship to clinical symptoms. *Psychiatry Res Neuroimaging* 2018;275:5–13 [Published correction appears in *Psychiatry Res Neuroimaging* 2019;286:76].
137. Burton EJ, McKeith IG, Burn DJ, Williams ED, O'Brien JT. Cerebral atrophy in Parkinson's disease with and without dementia: a comparison with Alzheimer's disease, dementia with Lewy bodies and controls. *Brain* 2004;127(Pt 4):791–800.
138. Tinaz S, Courtney MG, Stern CE. Focal cortical and subcortical atrophy in early Parkinson's disease. *Mov Disord* 2011;26(3):436–441.
139. Chen S, Tan HY, Wu ZH, et al. Imaging of olfactory bulb and gray matter volumes in brain areas associated with olfactory function in patients with Parkinson's disease and multiple system atrophy. *Eur J Radiol* 2014;83(3):564–570.
140. Cigdem O, Beheshti I, Demirel H. Effects of different covariates and contrasts on classification of Parkinson's disease using structural MRI. *Comput Biol Med* 2018;99:173–181.
141. Vasconcellos LF, Pereira JS, Adachi M, et al. Volumetric brain analysis as a predictor of a worse cognitive outcome in Parkinson's disease. *J Psychiatr Res* 2018;102:254–260.
142. Vitali P, Pan MI, Palesi F, et al. Substantia nigra volumetry with 3-T MRI in de novo and advanced Parkinson disease. *Radiology* 2020;296(2):401–410.
143. Benito-León J, Serrano JI, Louis ED, et al. Tremor severity in Parkinson's disease and cortical changes of areas controlling movement sequencing: A preliminary study. *J Neurosci Res* 2018;96(8):1341–1352.
144. Uribe C, Segura B, Baggio HC, et al. Cortical atrophy patterns in early Parkinson's disease patients using hierarchical cluster analysis. *Parkinsonism Relat Disord* 2018;50:3–9.
145. Goldman JG, Stebbins GT, Bernard B, Stoub TR, Goetz CG, deTolledo-Morrell L. Entorhinal cortex atrophy differentiates Parkinson's disease patients with and without dementia. *Mov Disord* 2012;27(6):727–734.
146. Mak E, Bergsland N, Dwyer MG, Zivadinov R, Kandiah N. Subcortical atrophy is associated with cognitive impairment in mild Parkinson disease: a combined investigation of volumetric changes, cortical thickness, and vertex-based shape analysis. *AJNR Am J Neuroradiol* 2014;35(12):2257–2264.
147. Filippi M, Canu E, Donzuso G, et al. Tracking cortical changes throughout cognitive decline in Parkinson's disease. *Mov Disord* 2020;35(11):1987–1998.
148. Gorges M, Kunz MS, Müller HP, et al. Longitudinal brain atrophy distribution in advanced Parkinson's disease: What makes the difference in “cognitive status” converters? *Hum Brain Mapp* 2020;41(6):1416–1434.
149. Goldman JG, Bledsoe IO, Merkitich D, Dinh V, Bernard B, Stebbins GT. Corpus callosal atrophy and associations with cognitive impairment in Parkinson disease. *Neurology* 2017;88(13):1265–1272.
150. Chagas MHN, Tumas V, Pena-Pereira MA, et al. Neuroimaging of major depression in Parkinson's disease: Cortical thickness, cortical and subcortical volume, and spectroscopy findings. *J Psychiatr Res* 2017;90:40–45.
151. Ma X, Su W, Li S, et al. Cerebellar atrophy in different subtypes of Parkinson's disease. *J Neurol Sci* 2018;392:105–112.
152. Goto M, Kamagata K, Hatano T, et al. Depressive symptoms in Parkinson's disease are related to decreased left hippocampal volume: correlation with the 15-item shortened version of the Geriatric Depression Scale. *Acta Radiol* 2018;59(3):341–345.
153. Shin JH, Shin SA, Lee JY, Nam H, Lim JS, Kim YK. Precuneus degeneration and isolated apathy in patients with Parkinson's disease. *Neurosci Lett* 2017;653:250–257.
154. Terada T, Miyata J, Obi T, Kubota M, Yoshizumi M, Murai T. Reduced gray matter volume is correlated with frontal cognitive and behavioral impairments in Parkinson's disease. *J Neurol Sci* 2018;390:231–238.
155. Radziunas A, Deltuva VP, Tamasauskas A, et al. Brain MRI morphometric analysis in Parkinson's disease patients with sleep disturbances. *BMC Neurol* 2018;18(1):88.
156. Campabadal A, Uribe C, Segura B, et al. Brain correlates of progressive olfactory loss in Parkinson's disease. *Parkinsonism Relat Disord* 2017;41:44–50.
157. Hossein-Tehrani MR, Ghaedian T, Hooshmandi E, Kalhor L, Foroughi AA, Ostovan VR. Brain TRODAT-SPECT Versus MRI morphometry in distinguishing early mild Parkinson's disease from other extrapyramidal syndromes. *J Neuroimaging* 2020;30(5):683–689.
158. Saeed U, Compagnone J, Aviv RI, et al. Imaging biomarkers in Parkinson's disease and Parkinsonian syndromes: current and emerging concepts. *Transl Neurodegener* 2017;6(1):8.
159. Sako W, Murakami N, Izumi Y, Kaji R. The difference in putamen volume between MSA and PD: evidence from a meta-analysis. *Parkinsonism Relat Disord* 2014;20(8):873–877.
160. Schulz JB, Skalej M, Wedekind D, et al. Magnetic resonance imaging-based volumetry differentiates idiopathic Parkinson's syndrome from

- multiple system atrophy and progressive supranuclear palsy. *Ann Neurol* 1999;45(1):65–74.
161. Massey LA, Micallef C, Paviour DC, et al. Conventional magnetic resonance imaging in confirmed progressive supranuclear palsy and multiple system atrophy. *Mov Disord* 2012;27(14):1754–1762.
 162. Brenneis C, Seppi K, Schocke MF, et al. Voxel-based morphometry detects cortical atrophy in the Parkinson variant of multiple system atrophy. *Mov Disord* 2003;18(10):1132–1138.
 163. Kim HJ, Jeon BS, Kim YE, et al. Clinical and imaging characteristics of dementia in multiple system atrophy. *Parkinsonism Relat Disord* 2013;19(6):617–621.
 164. Boxer AL, Geschwind MD, Belfor N, et al. Patterns of brain atrophy that differentiate corticobasal degeneration syndrome from progressive supranuclear palsy. *Arch Neurol* 2006;63(1):81–86.
 165. Brenneis C, Seppi K, Schocke M, Benke T, Wenning GK, Poewe W. Voxel based morphometry reveals a distinct pattern of frontal atrophy in progressive supranuclear palsy. *J Neurol Neurosurg Psychiatry* 2004;75(2):246–249.
 166. Padovani A, Borroni B, Brambati SM, et al. Diffusion tensor imaging and voxel based morphometry study in early progressive supranuclear palsy. *J Neurol Neurosurg Psychiatry* 2006;77(4):457–463.
 167. Price S, Paviour D, Scahill R, et al. Voxel-based morphometry detects patterns of atrophy that help differentiate progressive supranuclear palsy and Parkinson's disease. *Neuroimage* 2004;23(2):663–669.
 168. Lee Y, Lee DK, Lee JM, et al. Volumetric analysis of the cerebellum in patients with progressive supranuclear palsy. *Eur J Neurol* 2017;24(1):212–218.
 169. Reginold W, Lang AE, Marras C, Heyn C, Alharbi M, Mikulis DJ. Longitudinal quantitative MRI in multiple system atrophy and progressive supranuclear palsy. *Parkinsonism Relat Disord* 2014;20(2):222–225.
 170. Burton EJ, Barber R, Mukaetova-Ladinska EB, et al. Medial temporal lobe atrophy on MRI differentiates Alzheimer's disease from dementia with Lewy bodies and vascular cognitive impairment: a prospective study with pathological verification of diagnosis. *Brain* 2009;132(Pt 1):195–203.
 171. Nedelska Z, Ferman TJ, Boeve BF, et al. Pattern of brain atrophy rates in autopsy-confirmed dementia with Lewy bodies. *Neurobiol Aging* 2015;36(1):452–461.
 172. Shimizu S, Kanetaka H, Hirao K, et al. Neuroimaging for diagnosing dementia with Lewy bodies: What is the best neuroimaging technique in discriminating dementia with Lewy bodies from Alzheimer's disease? *Geriatr Gerontol Int* 2017;17(5):819–824.
 173. Colloby SJ, Elder GJ, Rabee R, O'Brien JT, Taylor JP. Structural grey matter changes in the substantia innominata in Alzheimer's disease and dementia with Lewy bodies: a DARTEL-VBM study. *Int J Geriatr Psychiatry* 2017;32(6):615–623.
 174. McKeith IG, Boeve BF, Dickson DW, et al. Diagnosis and management of dementia with Lewy bodies: Fourth consensus report of the DLB Consortium. *Neurology* 2017;89(1):88–100.
 175. Donaghy PC, Firbank MJ, Thomas AJ, et al. Clinical and imaging correlates of amyloid deposition in dementia with Lewy bodies. *Mov Disord* 2018;33(7):1130–1138.
 176. Schneider JA, Arvanitakis Z, Bang W, Bennett DA. Mixed brain pathologies account for most dementia cases in community-dwelling older persons. *Neurology* 2007;69(24):2197–2204.
 177. Mak E, Su L, Williams GB, et al. Progressive cortical thinning and subcortical atrophy in dementia with Lewy bodies and Alzheimer's disease. *Neurobiol Aging* 2015;36(4):1743–1750.
 178. Borroni B, Premi E, Formenti A, et al. Structural and functional imaging study in dementia with Lewy bodies and Parkinson's disease dementia. *Parkinsonism Relat Disord* 2015;21(9):1049–1055.
 179. Lee JE, Park B, Song SK, Sohn YH, Park HJ, Lee PH. A comparison of gray and white matter density in patients with Parkinson's disease dementia and dementia with Lewy bodies using voxel-based morphometry. *Mov Disord* 2010;25(1):28–34.
 180. Gazzina S, Premi E, Turrone R, et al. Subcortical matter in the α -synucleinopathies spectrum: an MRI pilot study. *J Neurol* 2016;263(8):1575–1582.
 181. Peraza LR, Colloby SJ, Firbank MJ, et al. Resting state in Parkinson's disease dementia and dementia with Lewy bodies: commonalities and differences. *Int J Geriatr Psychiatry* 2015;30(11):1135–1146.